J. Fluid Mech. (2000), *vol.* 404, *pp.* 179–209. Printed in the United Kingdom

Linear stability of free shear flows of fibre suspensions

By J. AZAIEZ

Department of Chemical and Petroleum Engineering, University of Calgary, Calgary, Alberta, Canada T2N 1N4

(Received 28 June 1999 and in revised form 27 September 1999)

A linear stability analysis of the mixing layer in the presence of fibre additives is presented. Using a formulation based on moments of the probability distribution function to determine the particle orientation, we extend the classical linear stability theory and derive a modified Orr–Sommerfeld equation. It is found that, for large Reynolds numbers, the flow instability is governed by two parameters: a dimensionless group H, analogous to a reciprocal Reynolds number representing the importance of inertial forces versus viscous forces associated with the anisotropic elongational viscosity of the suspension; and a coefficient C_I that accounts for inter-particle hydrodynamic interactions. A parametric study reveals that both parameters can induce an important attenuation of the flow instability. Furthermore, we show that the stabilizing effects arise from the orientation diffusion due to hydrodynamic interactions, and not from the anisotropy induced by the presence of fibres in the flow, as speculated before. The examination of profile contours of different perturbation terms and the analysis of the rate of production of enstrophy show clearly that the main factor behind the reduction of the flow instability is associated with the fibre shear stress disturbance. This disturbance acts as a dissipative term as the fibres, due to the orientational diffusivity arising from hydrodynamic interactions, deviate from the fully aligned anisotropic orientation. On the other hand, fibre normal stresses act as a destabilizing factor and are important only in the absence of hydrodynamic interactions.

1. Introduction

It is well known that small amounts of additives such as polymers, surfactants and solid or flexible particles can induce spectacular drag reduction effects in many turbulent flows. Extensive reviews such as those by Hoyt (1972) and Berman (1978) have documented a large number of experimental observations that provide evidence of the great potential of such additives in reducing turbulent effects.

Most of the existing literature dealing with drag reduction by additives has mainly focused on the use of polymer additives, particularly in wall-bounded flows, due to their importance in many technological processes (see for example Pinho & Whitelaw 1990, and Tiederman 1990). On the other hand, the use of fibre additives as potential drag-reducing agents remains very limited. Nevertheless, the results of experimental studies that have investigated pipe flows in the presence of particle additives showed drag reduction effects of up to 60% (Arranaga 1970). Depending on the flow geometry, the particles size and the importance of viscous effects versus inertial effects, the addition of fibres to a flow may be either stabilizing (Vaseleski & Metzner 1974) or destabilizing (Pilipenko, Kalinichenko & Lemak 1981). In general, where particle

additives tend to stabilize the flow, it has been observed that the stabilizing effect increases with the particle aspect ratio (length to diameter ratio) and with fibre concentration (Vaseleski & Metzner 1974).

Free shear flows such as mixing layers, jets and wakes differ from the previously mentioned wall-bounded flows in that they have an inflectional mean velocity profile, and hence are subject to inviscid instabilities. These flows are encountered in a wide variety of natural and technological systems and it is important to understand the mechanisms governing the process of transition to turbulence in order to predict, and if possible control, the evolution of such flows.

The stability of this class of flows in the presence of additives has been a concern but not a focus of previous studies, and only limited attention has been devoted to this problem. Among the few experimental investigations dealing with polymer and surfactant additives, we should mention the work of Gadd (1965) for the jet flow, and those of Hibberd, Kwade & Scharf (1982) and Riediger (1989) for the mixing layer, and Cadot & Lebey (1999) for the wake flow. These studies showed that the addition of polymers or surfactants leads to a suppression of the flow instability and an attenuation of small-scale turbulence. Such additives are also responsible for the delay in the formation of the typical structures of the plane mixing layer, i.e. roll-up and pairing. On the theoretical side, we mention the linear inertial instability studies of Azaiez & Homsy (1994*a*), and Rallison & Hinch (1995), and the full numerical simulations by Azaiez & Homsy (1994*b*) and Kumar & Homsy (1999). These studies allowed a better understanding of the mechanisms of stabilization and shed new light on the interactions between the flow and viscoelastic polymer additives.

There are much fewer experimental studies devoted to free shear flows of fibre suspensions. The experimental visualizations of the jet flow by Filipsson, Torgny Lagerstedt & Bark (1977) represent one of the few experiments devoted to the study of the stability of free shear flows in the presence of particle additives. The authors reported that the addition of a small amount of polymer (Polyox WSR-301) or fibres (asbestos) led to drastic changes in the flow that translated into an enhancement of large-scale turbulent structures and a modulation of the turbulence by the suppression of small-scale structures.

All existing experimental investigations of free shear flows with additives, whether viscoelastic substances or rigid particles, provide evidence of the great potential of such additives to reduce these flow instabilities. However, in spite of the overwhelming experimental and theoretical evidence for drag reduction by such additives, the physical mechanisms responsible for this phenomenon are not completely understood and remain a subject of debate. Many explanations have been proposed particularly for the role of polymer additives. The role of stress anisotropy due to polymer extension versus elasticity in the mechanism of drag reduction is still an ongoing subject of controversy. De Gennes (1990) and Joseph (1990), among other authors, suggest that elasticity is the main factor behind drag reduction by polymer additives. Other authors maintain that the main mechanism is associated with the anisotropy arising from the particular orientation of the polymer chains once they are fully stretched (Landahl 1972; Hinch 1977; Draad & Hulsen 1995).

Furthermore, the similarities observed between experimental studies involving polymer or fibre additives, and the fact that polymer chains undergoing strong strains may act hydrodynamically like solid particles, led many authors to speculate that these two additives modify flow instabilities in a similar manner. However for many reasons, we think that such analogies should not be taken too far. First, rigid particles lack the flexibility that polymer chains usually have and which may have important

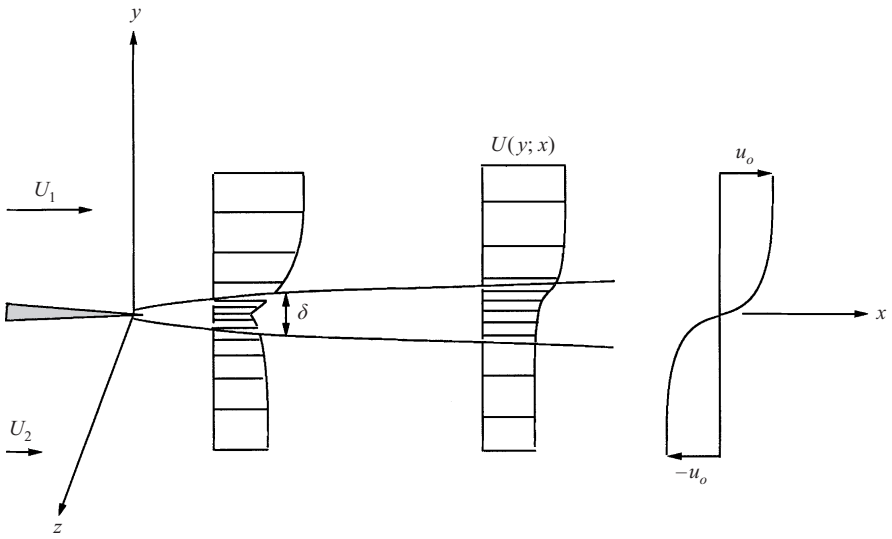

FIGURE 1. Schematic of the mixing layer.

hydrodynamic effects. Second, it is not obvious that a stretched polymer chain can retain its conformation without degradation, and therefore behave exactly like a long rigid particle. Furthermore, it is known that in general, for a given additive concentration, polymers tend to induce stronger drag reduction effects than their solid particle counterparts. Finally, experimental results such as those reported by Lee, Vaseleski & Metzner (1974) for pipe flows, show that the combined use of polymers and fibres leads to much larger drag reduction effects than usually obtained with either additive alone.

The objective of the present paper is to examine the linear stability of the mixing layer in the presence of fibre additives. This study is viewed as a logical extension to our previous work investigating the stability of the same flow in the presence of polymer additives (Azaiez & Homsy 1994*a*). We will focus on high but finite Reynolds number flows and examine the effects of different parameters such as fibre aspect ratio and volume fraction, as well as the role of hydrodynamic interactions. We will attempt to determine the mechanisms of stabilization or destabilization of the flow in relation to these parameters.

The paper is organized as follows. In the next section we present the equations used to determine the fibre orientation and the expression for their contribution to the total stress. The third section deals with the linearized equations describing the stability of the flow, and the fourth one presents the numerical methods used to solve these equations. The results of the stability analysis and the mechanisms of stabilization or destabilization of the flow are discussed in the fifth section.

2. Mathematical model

2.1. *Problem definition and Cauchy's laws of motion*

A schematic of the flow under consideration is shown in figure 1, where we have used the following notation: U_1 is the free-stream velocity in the upper flow; U_2 is the free-stream velocity in the lower flow; δ is the initial momentum thickness of the mixing layer. We assume without loss of generality that U_1 is larger than U_2 and

follow the flow in a Lagrangian reference frame moving with the average velocity $(U_1 + U_2)/2$. In this reference frame, the speed of the free-stream flow is denoted by $u_o = (U_1 - U_2)/2$. In all the subsequent analysis we denote by $\boldsymbol{i}$, $\boldsymbol{j}$ and $\boldsymbol{k}$ the unit vectors that point in the streamwise (x), transverse (y) and spanwise (z) directions, respectively and by $\boldsymbol{u} = (u, v, w)$ the velocity vector. The governing equations of the flow are

$$\nabla \cdot \boldsymbol{u} = 0, \tag{1}$$

$$\rho \left(\frac{\partial \boldsymbol{u}}{\partial t} + \boldsymbol{u} \cdot \nabla \boldsymbol{u} \right) = -\nabla p + \nabla \cdot \boldsymbol{\tau}. \tag{2}$$

In these equations, ρ is the fluid density, and p the isotropic pressure. The extra stress tensor $\boldsymbol{\tau}$ is decomposed as

$$\boldsymbol{\tau} = \boldsymbol{\tau}^s + \boldsymbol{\tau}^f. \tag{3}$$

The first term $\boldsymbol{\tau}^s$ corresponds to the contribution of the Newtonian suspending fluid to the total stress and is proportional to the rate of strain tensor $\dot{\boldsymbol{\gamma}} = (\nabla \boldsymbol{u} + \nabla \boldsymbol{u}^T)$, through the viscosity of the suspending fluid η, while the second term $\boldsymbol{\tau}^f$ represents the fibre contribution. In order to characterize the flow behaviour of the fibre suspension, we need to solve the equations for the conservation of mass and momentum, equations (1) and (2), in conjunction with an equation for the fibre stress $\boldsymbol{\tau}^f$. In the following section we discuss the approach we adopted to determine the expression for the fibre contribution to the total stress.

2.2. *Constitutive equations*

For a suspension of non-spherical rigid particles, the expression for the stress tensor in general depends on the details of the geometry of the particles, their volume fraction and orientation distribution. The present analysis will be limited to a suspension of monodisperse, neutrally buoyant rigid particles that are homogeneously distributed in the flow. In the following two subsections we present the formulations we used to determine the orientation of the fibres and their contribution to the total stress.

2.2.1. *Fibre orientation*

For a single particle, the orientation is usually described by a Fokker–Planck equation for the probability distribution function $\Gamma(\boldsymbol{p})$:

$$\frac{\partial \Gamma}{\partial t} + \nabla \cdot (\dot{\boldsymbol{p}} \Gamma - \boldsymbol{D}_r \cdot \nabla \Gamma) = 0, \tag{4}$$

where $\boldsymbol{p} = (p_i)$ is a unit vector denoting the orientation of the fibre, and $\Gamma(\boldsymbol{p})\mathrm{d}\boldsymbol{p}$ is the probability that a fibre be oriented between $\boldsymbol{p}$ and $\boldsymbol{p}+\mathrm{d}\boldsymbol{p}$. In the derivation of the above equation it is assumed that the suspending fluid is Newtonian and incompressible, and that particle inertia is negligible. This last assumption is equivalent to requiring that the Reynolds number based on the particles dimensions be small, i.e. $Re_f = u_o l/\nu \ll 1$ where l represents a characteristic dimension of the particles and ν is the kinematic viscosity of the suspending fluid.

The complexity and the usually prohibitively high computational cost associated with the use of equation (4) to describe particles orientation, have lead to many alternative approaches. The simplest approach is based on the aligned particle approximation, where one assumes that all particles align with the local velocity vector. In this approach, one solves only for the velocity field, which now plays the dual role of predicting the fluid motion and the particle orientation. This approach is

convenient to describe the flow of slender fibres in the absence of Brownian motion and fibre–fibre interactions, as the particles tend indeed to align with the streamlines. We will not adopt this approach in the present study since, as we shall see later, fibres are not perfectly aligned with the flow and their deviation from full alignment plays an important role in determining the stability of the flow.

A second approach, that we shall adopt here, uses orientation tensors defined as dyadic products of the unit vector $\boldsymbol{p}$ averaged over all possible orientations to describe the orientation of the fibres (Hinch & Leal 1976). In particular, a second-order and a fourth-order orientation moment $\langle \boldsymbol{pp} \rangle$ and $\langle \boldsymbol{pppp} \rangle$, are defined as follows:

$$\langle \boldsymbol{pp} \rangle = \oint p_i p_j \Gamma(\boldsymbol{p}) \mathrm{d}\boldsymbol{p}, \tag{5}$$

$$\langle \boldsymbol{pppp} \rangle = \oint p_i p_j p_k p_l \Gamma(\boldsymbol{p}) \mathrm{d}\boldsymbol{p}. \tag{6}$$

The equation of change for the second-order tensor $\langle \boldsymbol{pp} \rangle$ (Prager 1957; Hinch & Leal 1976) can be formulated as follows:

$$\langle \boldsymbol{pp} \rangle_{(1)} = \frac{\chi - 1}{2} [\dot{\gamma} . \langle \boldsymbol{pp} \rangle + \langle \boldsymbol{pp} \rangle . \dot{\gamma}] - \chi [\dot{\gamma} : \langle \boldsymbol{pppp} \rangle] + 2\boldsymbol{D}_r [\boldsymbol{I} - m \langle \boldsymbol{pp} \rangle], \tag{7}$$

where

$$\langle \boldsymbol{pp} \rangle_{(1)} = \frac{\partial \langle \boldsymbol{pp} \rangle}{\partial t} + \boldsymbol{u} \cdot \nabla \langle \boldsymbol{pp} \rangle - \nabla \boldsymbol{u}^T \cdot \langle \boldsymbol{pp} \rangle - \langle \boldsymbol{pp} \rangle \cdot \nabla \boldsymbol{u} \tag{8}$$

is the upper-convected derivative of $\langle \boldsymbol{pp} \rangle$. In the previous equations, $\boldsymbol{I}$ is the unit tensor, m is the dimension of the space and $\chi = (r^2 - 1)/(r^2 + 1)$ is a parameter related to the aspect ratio of the fibre $r = L/d = 2l/d$, where L and d represent the fibre characteristic length and thickness, respectively. In what follows we adopt the following more convenient notation:

$$\boldsymbol{a_2}(a_{ij}) = \langle \boldsymbol{pp} \rangle,$$
$$\boldsymbol{a_4}(a_{ijkl}) = \langle \boldsymbol{pppp} \rangle.$$

The equation for the development of the second-order orientation tensor $\boldsymbol{a_2}$ contains the unknown fourth-order orientation tensor $\boldsymbol{a_4}$. In general, the evolution equation for any order moment of $\boldsymbol{p}$ will involve the next higher-order moment. Therefore, to obtain a closed set of equations, one needs to determine $\boldsymbol{a_4}$ as a function of $\boldsymbol{a_2}$. A variety of closure approximations have been proposed to relate the second- and fourth-order orientation tensors; $\boldsymbol{a_4} = \mathscr{C}(\boldsymbol{a_2})$. Among these, we will mention the quadratic closure approximation which has been extensively used in the literature, and which, strictly speaking, is valid only for a perfectly aligned orientation distribution. Most of the available approximations, including the quadratic one, perform well only for some specific flow fields, and therefore cannot be used for a general complex flow. In the present study we will use the natural closure approximation that has been recently developed by Verleye & Dupret (1993). This closure approximation is based on an analytical solution for the orientation distribution function in the limit of high-aspect-ratio, non-Brownian fibres. Comparisons with exact results obtained by solving directly for the orientation distribution function, show that this closure gives remarkably excellent results for a large variety of flow fields (Cintra & Tucker 1995).

The natural closure approximation is frame invariant and has a simple analytical form only in the case of a two-dimensional orientation. However, there is no simple

formulation for a three-dimensional orientation distribution. For the purpose of the present study, we will use the analytical form of the closure which is strictly valid only for two-dimensional orientation, while in reality fibres may have an orientation component outside of the plane of the flow. We adopt the analytical form mainly for reasons of simplicity, and we believe that it will capture the essential physics of the two-dimensional flow investigated here.

For a two-dimensional orientation distribution ($m = 2$), the relation $\boldsymbol{a_4} = \mathscr{C}(\boldsymbol{a_2})$ based on the natural closure is

$$a_{ijkl} = \frac{\det(\boldsymbol{a_2})}{6}(\delta_{ij}\ \delta_{kl} + \delta_{ik}\ \delta_{jl} + \delta_{il}\ \delta_{jk}) + \tfrac{1}{3}(a_{ij}a_{kl} + a_{ik}a_{jl} + a_{il}a_{jk}), \tag{9}$$

where δ_{ij} is the usual Kronecker symbol and det is the determinant. From equation (9), one gets the following expressions for the term $\boldsymbol{F} = (\dot{\gamma} : \boldsymbol{a_4})$ appearing in the evolution equation for $\boldsymbol{a_2}$:

$$(\dot{\gamma} : \boldsymbol{a_4}) = \tfrac{1}{3}[(\det(\boldsymbol{a_2})\,\dot{\gamma} + \mathrm{tr}(\dot{\gamma}\cdot\boldsymbol{a_2})\,\boldsymbol{a_2} + 2(\boldsymbol{a_2}\cdot\dot{\gamma}\cdot\boldsymbol{a_2})]. \tag{10}$$

This last expression will be used later in deriving the linearized equations of the flow.

A last word must be said about the diffusion-like term in equation (4) which is analogous to the rotary motion of small Brownian particles. This term, containing an orientational diffusivity $\boldsymbol{D}_r$, accounts for general orientational diffusion resulting from inter-particle hydrodynamic interactions. In a typical flow of fibre suspensions, one may have to deal with many types of inter-particle interactions that can influence the physics of the flow. These interactions can be associated with hydrodynamic or colloidal forces, excluded volume and friction or direct particle–particle interactions. Accounting for all these interactions makes the determination of the expression for $\boldsymbol{D}_r$ a particularly delicate issue.

In the present study, we are interested in studying the role of pure hydrodynamic interactions, which we believe are the dominant type of interactions in the regime of concentrations we examine. The relevant previous studies by Rahnama, Koch & Shaqfeh (1995) and Koch (1995) showed that the orientational diffusivity depends on the fibre properties (shape and aspect ratio), the flow kinematics and the orientation distribution of the fibres. For a simple shear flow, $\boldsymbol{D}_r$ is in general not isotropic and scales like $(|\dot{\gamma}|\, n\, l^3/(r\, \ln^2(r))$, where n is the fibre number density, and $|\dot{\gamma}|$ is the scalar magnitude of the rate of strain tensor $\dot{\gamma}$,

$$|\dot{\gamma}| = \sqrt{\tfrac{1}{2}\,\mathrm{tr}(\dot{\gamma}\cdot\dot{\gamma})} = \sqrt{\tfrac{1}{2}\dot{\gamma}_{ij}\dot{\gamma}_{ji}}. \tag{11}$$

We should stress that the term $\boldsymbol{D}_r$ considered here is not associated with Brownian motion but is a hydrodynamically induced diffusivity that accounts for hydrodynamic interactions between the fibres.

In an earlier study, Folgar & Tucker (1984) suggested a simple expression where the diffusivity tensor $\boldsymbol{D}_r$ is assumed to be isotropic and is formulated as $C_I|\dot{\gamma}|$. The interaction coefficient C_I depends in general on the fibre concentration, shape, and aspect ratio. In this study we will adopt this last simplified formulation.

It is reasonable to expect that some physical aspects of the flow may be lost by disregarding the anisotropic nature of the diffusivity and its dependence on the fibre orientation distribution, and by using the orientation-tensor formulation instead of solving exactly for the probability distribution function $\Gamma(\boldsymbol{p})$. Furthermore, the fibres may have an orientation component off the plane of the flow that the present model does not account for. In spite of these simplifications, we believe that the present

formulation incorporates the essential physics and has the advantage of allowing a qualitative determination of the main effects of fibres on the flow dynamics without requiring complex and prohibitively expensive calculations.

2.2.2. *Fibre stress*

Several constitutive models have been developed to determine the expression for the fibre contribution to the bulk stress tensor $\boldsymbol{\tau}^f$. All these models whether derived from slender-body theory (Batchelor 1970, Hinch & Leal 1975; 1976) or by invoking continuum mechanics theory (Ericksen 1960), lead to a general expression of the form

$$\boldsymbol{\tau}^f = \eta\phi[A\,(\dot{\boldsymbol{\gamma}} : \boldsymbol{a_4}) + B\,(\dot{\boldsymbol{\gamma}} \cdot \boldsymbol{a_2} + \boldsymbol{a_2} \cdot \dot{\boldsymbol{\gamma}}) + C\,\dot{\boldsymbol{\gamma}} + \boldsymbol{D}\,\boldsymbol{a_2}]. \tag{12}$$

The material constants A, B, C and D may depend on the fibre properties and volume fraction, ϕ. Different models, either for dilute systems where the average fibre spacing is larger than the fibre length ($n\,l^3 \ll 1$), or semi-dilute systems where the average fibre spacing may vary between the fibre length and diameter ($nl^3 \gg 1$ and $nld^2 \ll 1$), lead to different expressions for the constants. In general, for suspensions that have weak or no Brownian motion, the fourth term ($\boldsymbol{D}\,\boldsymbol{a_2}$) can be neglected. Furthermore for large-aspect-ratio particles, B is much smaller than A and C, and the fibre stress can be written as

$$\boldsymbol{\tau}^f = \eta\,\phi[A\,(\dot{\boldsymbol{\gamma}} : \boldsymbol{a_4}) + C\,\dot{\boldsymbol{\gamma}}]. \tag{13}$$

For slender cylindrical fibres, it was found that C is equal to 2 (Giesekus 1962).

Batchelor (1971) used slender-body theory to determine the expression for A for the extensional flow of a suspension of rigid particles. In the dilute regime, Batchelor showed that the parameter A can be determined from the following relation:

$$A\phi \equiv \frac{2\pi\,nl^3}{3\ln(2r)} f(\epsilon). \tag{14}$$

The shape factor function $f(\epsilon)$ accounts for the finite aspect ratio of the fibre, and is equal to 1 for infinitely long fibres. For a finite-aspect-ratio fibre, $f(\epsilon)$ is

$$\left.\begin{aligned} f(\epsilon) &= \frac{1 + 0.64\epsilon}{1 - (K + \frac{3}{2})\epsilon} + [0.699 + 0.64(K + \tfrac{3}{2})]\epsilon^2 + o(\epsilon^2), \\ \epsilon &= \frac{1}{\ln(2r)}. \end{aligned}\right\} \tag{15}$$

The parameter K is zero for a fibre of circular cross-section. Batchelor (1971) showed that the previous formulation for A can be extended to the semi-dilute regime, and suggested the following expression:

$$A\phi \equiv -\frac{2\pi\,nl^3}{3\ln\left(\frac{1}{2}\sqrt{nld^2}\right)}. \tag{16}$$

Shaqfeh & Frederickson (1990) included inter-particle interactions in the expression for the viscosity for semi-dilute suspensions, and derived a more accurate expression:

$$A\phi \equiv \frac{4\,\pi\,nl^3}{3[\ln(1/\phi) + \ln(\ln(1/\phi)) + E(\phi)]}, \tag{17}$$

where $E(\phi)$ is of order 1 in the limit $\phi \to 0$. The authors determined limiting values of E in the two special cases of aligned and random fibres.

Regardless of the expression for A adopted, $\boldsymbol{\tau}^f$ should be regarded as the anisotropic

contribution of the particles to the extra-stress tensor. In a general flow, a long thin particle tends to resist stretching along its axis and the term $A\phi$ represents the importance of this resistance.

In the remainder, we focus on a suspension of cylindrical particles mainly in the semi-dilute regime, $(1/r^2 \ll \phi \ll 1/r)$, and use the following equivalent expressions for (16) and (17):

$$\text{Batchelor (1971)} : A \equiv \frac{r^2}{3\ln(\sqrt{2\pi/\phi})}; \tag{18}$$

$$\text{Shaqfeh \& Frederickson (1990)} : A \equiv \frac{2r^2}{3[\ln(1/\phi) + \ln(\ln(1/\phi)) + E(\phi)]}. \tag{19}$$

For aligned cylindrical particles, Shaqfeh & Frederickson (1990) found that $E(\phi)$ is equal to 0.1585. Since we are dealing with large-aspect-ratio particles that will be more or less aligned in the direction of the flow, we will adopt this value of E throughout this analysis.

3. Linearized equations

Using u_o and δ as the reference speed and the reference length respectively, the flow is characterized by the Reynolds number $Re = \rho\delta u_o/\eta = \delta u_o/v$, where v is the kinematic viscosity of the fluid. The other parameters of interest are the fibre volume fraction ϕ, aspect ratio re, and interaction coefficient C_I. The dimensionless equations expressed in terms of the vorticity ω and the second-order orientation tensors $\boldsymbol{a_2}$ are

$$\left.\begin{aligned} \frac{\partial\omega}{\partial t} + (\boldsymbol{u}\cdot\nabla\omega) &= \frac{1+C\phi}{Re}\nabla^2\omega + \frac{A\phi}{Re}[\boldsymbol{k}\cdot\nabla\times(\nabla\cdot\boldsymbol{F})], \\ \boldsymbol{a}_{2(1)} &= \frac{\chi-1}{2}(\dot{\boldsymbol{\gamma}}\cdot\boldsymbol{a_2} + \boldsymbol{a_2}\cdot\dot{\boldsymbol{\gamma}}) - \chi\boldsymbol{F} + 2C_I|\dot{\boldsymbol{\gamma}}|(\boldsymbol{I} - m\boldsymbol{a_2}), \\ \boldsymbol{F} &= (\dot{\boldsymbol{\gamma}} : \boldsymbol{a_4}), \\ \boldsymbol{a_4} &= \mathscr{C}(\boldsymbol{a_2}). \end{aligned}\right\} \tag{20}$$

By examining the right-hand side terms in the vorticity equation, it becomes clear that, for large Reynolds numbers, the contribution of the first term responsible for the diffusion of momentum is negligible compared to that of the second term as long as the term $(A\phi)$ is at least of the same order as Re. One can see from equation (16) or equation (17) that this is possible only if one considers high-aspect-ratio fibres. In this case, the equation for the second-order orientation tensor $\boldsymbol{a_2}$ will not depend explicitly on the aspect ratio r since the parameter $\chi = (r^2-1)/(r^2+1)$ is almost equal to one. As a consequence, for a high Reynolds number flow of a suspension of high-aspect-ratio fibres, the instability is governed by only two parameters: the interaction coefficient C_I and the parameter $A\phi/Re$, that we shall refer to as H. This conclusion will be checked in § 5 where we shall present a physical interpretation of the dimensionless group H.

We examine the stability of the flow by disturbing the base flow infinitesimally, and limit the analysis to the case of a two-dimensional flow ($m = 2$). For the parallel flow of a Newtonian fluid, the theorem of Squire (1933) states that two-dimensional disturbances are temporally more unstable than three-dimensional disturbances, and an investigation of two-dimensional disturbances is sufficient to determine the critical Reynolds number. It was not possible to derive an equivalent Squire theorem for

the flow of the fibre suspension examined in this study, and therefore the issue of three-dimensional linear stability is left an open problem.

For the base state, we assume that the laminar flow is quasi-parallel, i.e. that its variation is entirely in the direction normal to the flow. The parallel flow assumption is a satisfactory first approximation for treating the linear stability of viscous flows at sufficiently high *Re* (see Ling & Reynolds 1973). In Appendix A, we analyse the correction to the laminar flow of a Newtonian fluid due to the presence of non-interacting fibres ($C_I = 0$). In this analysis we show that, using a quadratic closure (Cintra & Tucker 1995), the expansion leads to an equivalent Blasius problem, and that the base-state flow profile can be mapped into the Blasius profile. Since solutions for the mixing layer are known to be closely approximated by the *tanh* velocity profile, we conclude that this profile is also satisfactory for the purpose of the present analysis. With this assumption, we take the base flow as

$$\left.\begin{aligned} U_o(y) &= \tanh(y), \\ \omega_o(y) &= \tanh^2(y) - 1, \quad \Psi_o(y) = \ln[\cosh(y)], \end{aligned}\right\} \tag{21}$$

where $U_o(y)$ is the base-state streamwise velocity, $\omega_o(y)$ the spanwise vorticity and $\Psi_o(y)$ the corresponding streamfunction expressed in dimensionless form. Note that (21) is a solution of the Cauchy equation provided that there is a dimensionless body force to balance the contribution of the fibre stress.

The components of the base-state orientation tensor $\boldsymbol{a_{2o}}$ are given by (see Appendix B):

$$a_{o11} = \frac{\chi + 1 - \beta}{2\chi}, \quad a_{o22} = \frac{\chi - 1 + \beta}{2\chi}, \quad a_{o12} = \frac{2C_I(1-\beta)}{\chi\beta},$$
$$\beta = \sqrt{\frac{1 - 16{C_I}^2 - \chi^2 + \sqrt{(16{C_I}^2 + \chi^2 - 1)^2 + 64{C_I}^2}}{2}},$$

and the corresponding components of the term $\boldsymbol{F_o} = (\dot{\boldsymbol{\gamma}}_o : \boldsymbol{a_{4o}})$ giving the-base state stress are

$$F_{o11} = 2a_{o12}\,a_{o11}\frac{\mathrm{d}U_o}{\mathrm{d}y}, \quad F_{o12} = (a_{o11}\,a_{o22} + a_{o12}^2)\frac{\mathrm{d}U_o}{\mathrm{d}y}, \quad F_{o22} = 2a_{o12}\,a_{o22}\frac{\mathrm{d}U_o}{\mathrm{d}y}.$$

In the special limit of zero orientational diffusivity, $C_I = 0$, the above expressions reduce to

$$a_{o11} = \frac{1}{2} + \frac{1 - \sqrt{1-\chi^2}}{2\chi}, \quad a_{o22} = \frac{1}{2} - \frac{1 - \sqrt{1-\chi^2}}{2\chi}, \quad a_{o12} = 0,$$

and

$$F_{o11} = F_{o22} = 0, \quad F_{o12} = a_{o11}\,a_{o22}\frac{\mathrm{d}U_o}{\mathrm{d}y}.$$

We now assume that the base flow is disturbed such that the vorticity, velocity, and orientation tensor are represented by the base-state profile plus a small perturbation:

$$\left.\begin{aligned} \omega(x,y,t) &= \omega_o(y) + \omega^*(x,y,t), \\ \boldsymbol{u}(x,y,t) &= U_o(y)\boldsymbol{i} + \boldsymbol{u}^*(x,y,t), \\ \boldsymbol{a_2}(x,y,t) &= \boldsymbol{a_{2o}}(y) + \boldsymbol{a_2^*}(x,y,t), \\ \boldsymbol{F}(x,y,t) &= \boldsymbol{F_o}(y) + \boldsymbol{F}^*(x,y,t), \end{aligned}\right\} \tag{22}$$

where the first-order perturbation term $\boldsymbol{F}^*$ is:

$$\left.\begin{aligned} \boldsymbol{F}^* = & \frac{\det(\boldsymbol{a_{2o}})}{3}\dot{\boldsymbol{\gamma}}^* - \frac{f^*}{12}\dot{\boldsymbol{\gamma}}_o + \frac{\mathrm{tr}(\dot{\boldsymbol{\gamma}}^* \cdot \boldsymbol{a_{2o}} + \dot{\boldsymbol{\gamma}}_o \cdot \boldsymbol{a_2^*})}{3}\boldsymbol{a_{2o}} + \frac{\mathrm{tr}(\dot{\boldsymbol{\gamma}}_o \cdot \boldsymbol{a_{2o}})}{3}\boldsymbol{a_2^*} \\ & + \tfrac{2}{3}(\boldsymbol{a_{2o}} \cdot \dot{\boldsymbol{\gamma}}_o \cdot \boldsymbol{a_2^*} + \boldsymbol{a_{2o}} \cdot \dot{\boldsymbol{\gamma}}^* \cdot \boldsymbol{a_{2o}} + \boldsymbol{a_2^*} \cdot \dot{\boldsymbol{\gamma}}_o \cdot \boldsymbol{a_{2o}}), \\ f^* = & -4(a_{o11}a_{22}^* + a_{o22}a_{11}^* - 2\,a_{o12}a_{12}^*). \end{aligned}\right\} \tag{23}$$

The perturbation terms are substituted into the system of equations (20) which are linearized in the usual way:

$$\frac{\partial \omega^*}{\partial t} + U_o\frac{\partial \omega^*}{\partial x} + v^*\,\omega_o' = \frac{1 + C\phi}{Re}\nabla^2\omega^* + H\left[\left(\frac{\partial^2}{\partial x^2} - \frac{\partial^2}{\partial y^2}\right)F_{12}^* + \frac{\partial^2(F_{22}^* - F_{11}^*)}{\partial x \partial y}\right], \tag{24a}$$

$$\frac{\partial a_{11}^*}{\partial t} + U_o\frac{\partial a_{11}^*}{\partial x} + v^*\,a_{o11}' = -4C_I U_o' a_{11}^* + 2C_I|\dot{\boldsymbol{\gamma}}^*|(1 - 2a_{o11}) + 2\chi\frac{\partial u^*}{\partial x}a_{o11} + \left[\chi\left(\frac{\partial u^*}{\partial y} + \frac{\partial v^*}{\partial x}\right) + \left(\frac{\partial u^*}{\partial y} - \frac{\partial v^*}{\partial x}\right)\right]a_{o12} + (1 + \chi)U_o' a_{12}^* - \chi F_{11}^*, \tag{24b}$$

$$\frac{\partial a_{12}^*}{\partial t} + U_o\frac{\partial a_{12}^*}{\partial x} + v^*\,a_{o12}' = -4C_I U_o' a_{12}^* - 4C_I|\dot{\boldsymbol{\gamma}}^*|a_{o12} - \left(\frac{\partial u^*}{\partial y} - \frac{\partial v^*}{\partial x}\right)a_{o11} - U_o' a_{11}^* + \frac{\chi}{2}\left(\frac{\partial u^*}{\partial y} + \frac{\partial v^*}{\partial x}\right) + \frac{1}{2}\left(\frac{\partial u^*}{\partial y} - \frac{\partial v^*}{\partial x}\right) - \chi F_{12}^*. \tag{24c}$$

To derive the previous expressions, we have used the following relations:

$$a_{o11} + a_{o22} = 1, \quad a_{11}^* + a_{22}^* = 0. \tag{25}$$

In the above equations, the prime symbol denotes the derivative with respect to y of base-state functions i.e. $X_o' = \boldsymbol{D}X_o = \mathrm{d}X_o/\mathrm{d}y$.

Since the base-state depends only on the transverse component y, we can use a normal mode analysis of the perturbation where the disturbances have the following form:

$$\omega^*(x, y, t) = \omega(y)\,\mathrm{e}^{\mathrm{i}\alpha(x - ct)},$$
$$\boldsymbol{a_2^*}(x, y, t) = \boldsymbol{a_2}(y)\,\mathrm{e}^{\mathrm{i}\alpha(x - ct)}, \text{etc.}$$

In the present study we focus on the temporal stability and take the wavenumber α to be real, while c is in general complex. The complex wave speed is written as $c = c_r + \mathrm{i}c_i$, where c_r is the propagation velocity and c_i is a measure of the rate of amplification of the disturbance. The growth rate of the disturbance is then defined as $\sigma = \alpha c_i$. Using the above equations, we extended the classical linear stability analysis to include the effects of fibre additives, and obtained the following modified Orr–Sommerfeld equation (see Appendix C):

$$\sum_{i=0}^{4} J_i(y)\mathrm{D}^i\psi = 0 \tag{26}$$

with the boundary conditions:

$$\left.\begin{array}{rl} \psi \to 0 & \text{as} \quad y \to \pm\infty \\ \mathrm{D}\psi \to 0 & \text{as} \quad y \to \pm\infty. \end{array}\right\} \tag{27}$$

4. Solution of the eigenvalue problem

Following the usual Newtonian development, we assume that $\psi_r = \mathrm{Re}(\psi)$ is an even function of y while $\psi_i = \mathrm{Im}(\psi)$ is an odd function of y. Thus the domain of integration can be reduced to the upper half of the flow $[0, +\infty]$. Furthermore, we assume that the instability wave travels with the mean velocity. This assumption was verified by the finite difference method which makes no *a priori* assumption about c_r, and which showed that for all the eigenvalue problems we solve, $c_r = 0$ for the largest c_i.

In order to check the validity of the numerical results and to ensure that we obtained the whole set of solutions, we used three methods to solve the linearized problem with the appropriate boundary conditions. The first one consists of an iterative method based on orthogonal shooting which has been described in detail in Azaiez & Homsy (1994*a*). The second method is based on a multiple shooting technique (Ascher, Mattheij & Russel 1988). In this method one divides the whole interval by a mesh into N sub-intervals and shoots in each interval. The final result is obtained from the different solutions in the sub-intervals by imposing matching conditions at the shooting points. This method is very useful when the problem has both rapidly decaying and rapidly growing solutions. In the third method, we solved the linearized vorticity and fibre orientation equations using the finite difference method (Azaiez & Homsy 1994*a*). The ordinary differential equations are transformed into a set of finite difference equations and lead to a generalized eigenvalue problem $\boldsymbol{AX} = \lambda \boldsymbol{BX}$ which was solved using a standard QR algorithm.

For all three methods, the accuracy of the results was tested by refining the mesh and varying the width of the domain in the transverse direction $[0, \mathrm{Y}]$. At small wavenumbers, a large shooting distance Y was usually required because of the slow decay of the eigenfunctions. Furthermore, we used double precision arithmetic which allowed computation of even weakly amplified unstable modes, and checked that each method reproduced the well-known calculations for a pure Newtonian fluid (Michalke 1964).

5. Results

In the previous sections we developed a modified Orr–Sommerfeld equation that describes the linear stability of the mixing layer in the presence of fibre additives. In what follows, we will present instability characteristics obtained from the numerical solution of this equation.

5.1. *Instability characteristics*

In a first stage we will disregard the effects of the orientational diffusivity, and fix the value of the interaction coefficient C_I to 0.01. In practical terms, it is difficult to determine experimentally an accurate value of the orientational diffusivity or equivalently the parameter C_I. The value of C_I adopted here, though arbitrary due to the lack of accurate experimental data, falls within the range of values reported in earlier studies (see for example Folger & Tucker 1984 and Rahnama *et al.* 1995).

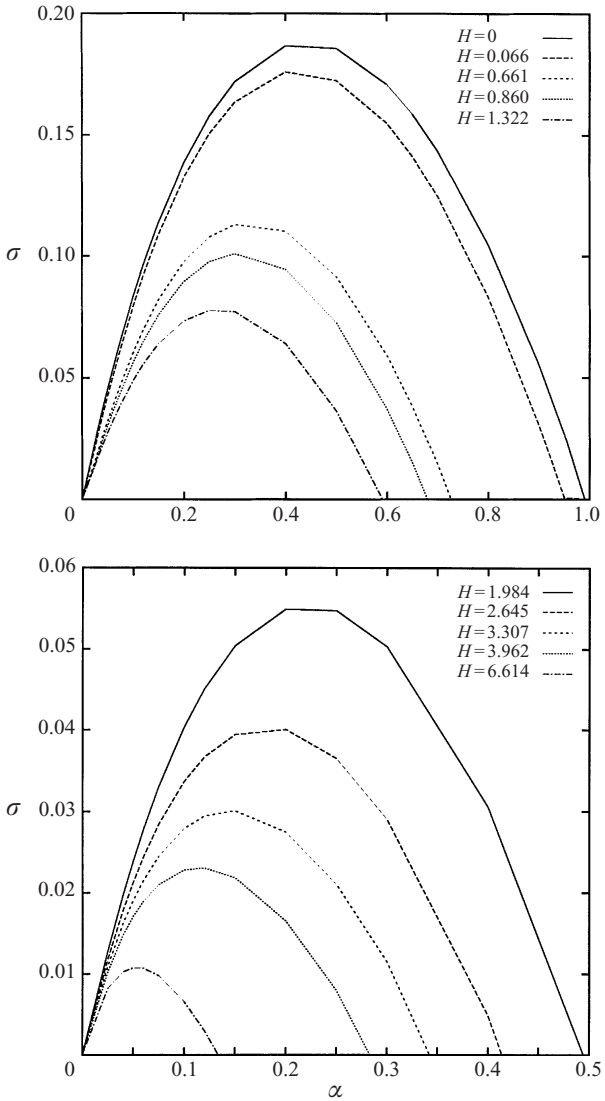

FIGURE 2. Instability characteristics for different values of H and $C_I = 0.01$.

Furthermore, unless stated otherwise, we take the Reynolds number equal to 10^3. This value is of the same order of magnitude as the values reported in the experimental study of Filipsson *et al.* (1977).

We conducted numerical simulations for different values of the fibre volume fraction and aspect ratio. The results of these simulations showed that fibre additives reduce the flow instability if the particles are of large aspect ratio, and their volume fraction is high, while still remaining within the semi-dilute limit for which the model is valid. As anticipated, it was also found that the flow instability does not depend separately on the values of r, ϕ and Re, nor on the exact expression for the parameter A, but only on the value of the dimensionless group H introduced earlier.

Strictly speaking, this last result is valid as long as the viscous term in the vorticity equation can be neglected (say $Re \geqslant 10^3$) and the fibres have a large aspect ratio (say

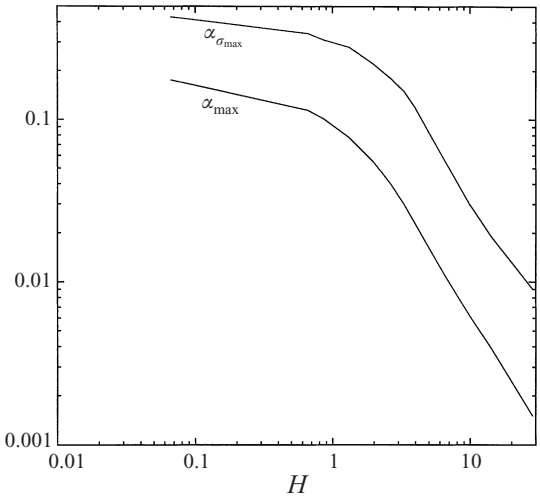

FIGURE 3. Variations of the maximum growth rate and the corresponding wavenumber with H for $C_I = 0.01$.

$r \geqslant 10^2$). In the remainder of this study, we shall consider a high Reynolds number flow in the presence of high-aspect-ratio fibres, and use H as the main parameter to describe the flow instability.

From our previous interpretation of the term $A\phi$ as the ratio of the extensional viscosity of the suspension and the shear viscosity, one can regard the parameter $H = A\phi/Re$ as the inverse of a Reynolds number based on the anisotropic elongational viscosity of the suspension, i.e. $H \equiv 1/Re_{el} \equiv \eta_{el}/\rho\delta u_o$. In the absence of fibres, H is identically zero, while for fibre-laden flows, H is proportional to the particle elongational viscosity and reflects the degree of resistance of a fibre to a stretching flow.

Figure 2 shows the variation of the growth rate of the disturbance σ versus the wavenumber α for different values of the parameter H and for $C_I = 0.01$. The curve corresponding to $H = 0$ represents the Newtonian limit (no fibres) and reproduces previous results with the maximum growth rate occurring at a wavelength $\alpha \sim 0.44$ (Azaiez 1993). As H is increased, the flow instability is substantially modified. The region of unstable wavenumbers is reduced from that of the pure Newtonian flow, and the entire unstable spectrum is shifted towards longer waves. Furthermore, the largest growth rate that governs the instability of the flow is substantially reduced. This result suggesting that fibres tend to stabilize the shortest waves is in agreement with the observations of Filipsson *et al.* (1977) who reported an increase in the wavelength of the flow turbulent structures. This attenuation of the instability suggests the presence of a mechanism of stabilization that we shall discuss later.

The previous results show conclusively that fibre additives reduce considerably the flow instability when the parameter H becomes large. However, one may ask if the flow can be totally stabilized for large enough values of H. Since it was not possible to conduct an asymptotic analysis for large H, we have simply plotted the variation of the maximum growth rate σ_{max} and the corresponding wavenumber $\alpha_{\sigma_{max}}$ versus the parameter H. Using a logarithmic scale, we show in figure 3 the variations of σ_{max} and $\alpha_{\sigma_{max}}$ versus H. From this figure one can see that, for large values of H, the decay of both σ_{max} and $\alpha_{\sigma_{max}}$ with H can be closely described by a power law. An

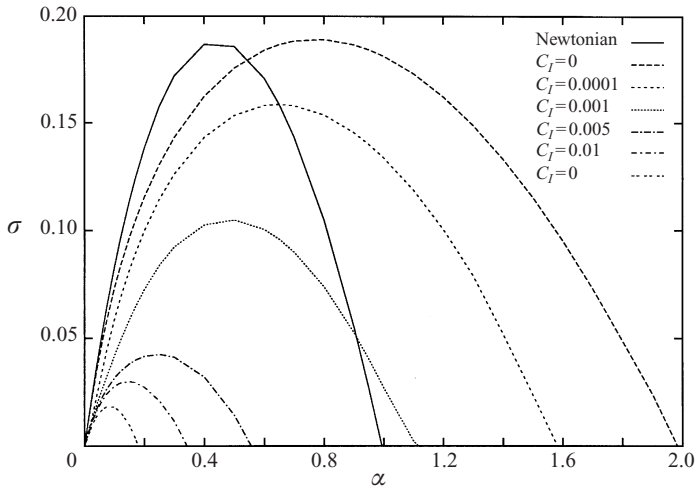

FIGURE 4. Instability characteristics as a function of C_I: $H = 3.31$.

interpolation of the numerical data shows that the maximum growth rate decays like $H^{-1.42}$. This last result indicates that the addition of fibres reduces the flow instability without completely suppressing it, which is similar to what we have reported for the viscoelastic mixing layer (Azaiez & Homsy 1994*a*).

5.2. *Role of fibre–fibre interactions*

An important question that arises in the study of flows of fibre suspensions is related to the interactions between the disturbance fields of the different particles, i.e. the problem of hydrodynamic interactions. In this section, we will investigate this question by fixing all parameters except C_I.

Figure 4 depicts instability characteristics for $H = 3.31$ and various values of C_I. It is clear from this figure that, for large interaction coefficients, an increase in C_I reduces the instability of the flow in a similar way to what was reported in the previous section when H is increased. There is however a fundamental difference for small values of the interaction coefficient. Indeed, for very small but non-zero values of C_I, the fibre suspension flow is, strictly speaking, less unstable than its Newtonian counterpart since the maximum growth rate has decreased. However, the spectrum of unstable wavenumbers is much larger than in the Newtonian case. Furthermore, when hydrodynamic interactions are disregarded ($C_I = 0$), the maximum growth rate becomes slightly larger than for the Newtonian fluid and the spectrum of unstable wavenumbers is almost doubled. From this last result, one should expect a fibre-laden flow to be unstable to higher frequency disturbances than its Newtonian counterpart. This means that such flows will show a stronger presence of fine turbulent structures when no or very weak hydrodynamic interactions are present in the flow. However, the experimental results of Filipsson *et al.* (1977) for the jet flow of fibre suspensions show just the opposite. This suggests that hydrodynamic interactions are not only important in the flow and therefore cannot be omitted in the analysis, but most importantly they are a key factor in the reduction of the flow instability. As we have mentioned earlier, exact values of the orientational diffusivity are not easy to determine. However, the present study suggests that, with the model adopted here,

values of the order of 0.01 or larger lead to predictions that are in better qualitative agreement with the experimental observations.

A final important question that may arise from the previous observations, is how does the present model behave in the dilute regime where hydrodynamic interactions can be neglected. We ran a few simulations using equation (14) valid in the dilute regime, for $Re = 10^3$, $r = 10^3$, $\phi = 10^{-6}$ which correspond to $H \approx 5 \times 10^{-5}$, and examined the effects of varying C_I between 0.1 and zero. Even though a value of C_I of the order of 0.1 is unrealistically high for a dilute solution, it was found that, for all the values of C_I examined, the instability characteristics were virtually identical to that of the Newtonian fluid. This can be explained by the fact that H is extremely small, and therefore the effects of fibres on the flow will not be significant. Furthermore, this result shows that the present model does indeed reflect the real behaviour of the fluid, and that the effects of hydrodynamic interactions on the flow instability are noticeable only in the semi-dilute regime.

5.3. *Mechanisms of stabilization*

In this section we will attempt to determine the mechanisms responsible for the reduction of the flow instability reported earlier. We present results based on the eigenfunctions obtained from the solution of the modified Orr–Sommerfeld equation. From the unstable eigenvalues, we select the one corresponding to the largest growth rate and normalize the corresponding eigenfunction such that $\psi_r(0) = 1$. All other disturbance functions $\omega, \boldsymbol{F}, \boldsymbol{a_2}$, etc. can then be easily determined.

Figure 5 depicts the variations of the real and imaginary parts of the eigenfunction ψ for different values of the parameter H. For illustrative purposes, we plot as a thick solid line a function proportional to the base-state velocity $U_o = \tanh(y)$ to show the extent of the shear layer. Furthermore, to present clearly the behaviour of the disturbance function close to the shear layer, we show the variation over only a fraction of the extent of the computational domain in the transverse direction.

For the Newtonian fluid ($H = 0$), most of the contribution of the eigenfunction lies within the shear layer region and decreases rapidly outside this region. As H is increased, the eigenfunction for interacting fibres ($C_I = 0.01$) extends beyond the shear layer and shows a slower decay with the transverse position y. Furthermore, the transverse location at which the eigenfunction reaches its maximum shifts away from the shear layer. When the effects of hydrodynamic interactions are ignored, the eigenfunction shows a very sharp increase, reaches its maximum within the shear layer, and then decays rapidly outside the shear layer. Note that the results described above are valid for both the real and imaginary parts of the eigenfunction.

A physical interpretation of these results can be obtained by recalling the relationship between the velocity vector and the streamfunction. The transverse component of the velocity disturbance, which is a key indicator of the strength of the subsequent roll-up of the flow, is related to the streamfunction through the relation $v = -\mathrm{i}\alpha\psi$. From the previous remarks, we conclude that in the cases of the Newtonian fluid and the non-interacting fibres, the contribution of v is mainly concentrated within the shear layer where the base-state velocity U_o is very small. This is indicative of a potentially strong effect of the transverse velocity disturbance on the flow. Furthermore, the sharp gradient within the shear layer of the eigenfunction for $C_I = 0$ suggests a strong contribution of the streamwise velocity disturbance $u = \partial\psi/\partial y$ in this region of the flow. On the other hand, for interacting fibres with large H, the maximum of v lies outside the shear layer. This contribution of the transverse velocity disturbance,

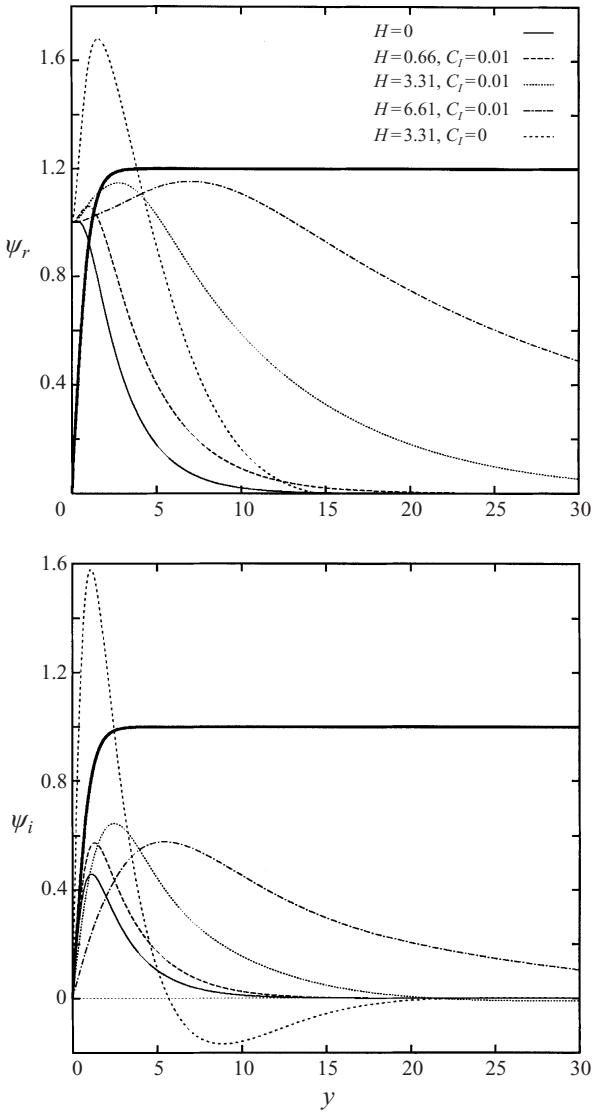

FIGURE 5. Variation of the real and imaginary parts of the eigenfunction.

in a region of the flow where the fluid moves at the free-stream velocity, probably will not have important effects on the flow instability.

Figure 6 shows the variations of the real parts of the two components of the orientation tensor disturbance, $\boldsymbol{a_2}$. A look at the figure for the component a_{11}, representing the effects on the degree of alignment with the flow, reveals that this component decreases sharply with H when $C_I = 0.01$. Furthermore, the disturbance decay is slower, and its contribution extends far beyond the shear layer for larger H. In the case where hydrodynamic interactions are not considered, the contribution of the disturbance a_{11} is mainly restricted to the shear layer and decays rapidly outside of this region. Similar qualitative results are obtained for a_{12} with the important exception that the a_{12} perturbation is almost two order of magnitudes larger than that of a_{11}.

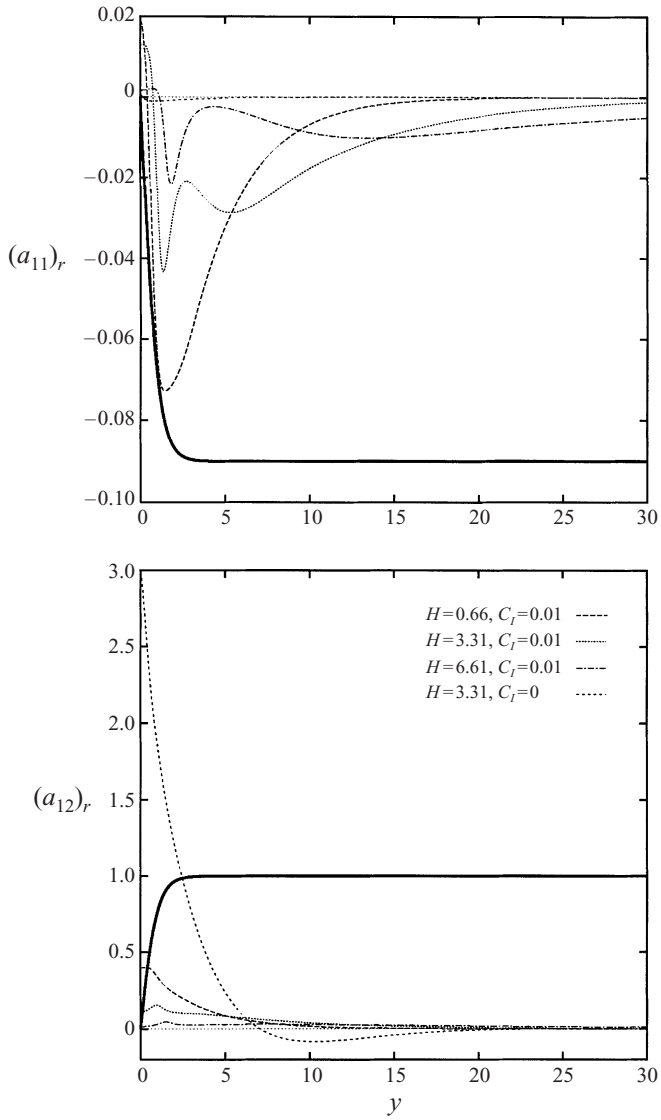

FIGURE 6. Variation of the two components of the disturbance of the second-order orientation tensor.

To understand the role of the interaction coefficient, let us examine the special case of infinitely long fibres ($re \to \infty, \chi = 1$), and consider a flow where hydrodynamic interactions are very weak. In this case, it is possible to get an expansion for the components of the base-state orientation tensor in terms of C_I:

$$a_{o11} = 1 - {C_I}^{1/2} + {C_I}^{3/2} + o({C_I}^{3/2}),$$

$$a_{o12} = {C_I}^{1/2} - 2C_I + {C_I}^{3/2} + o({C_I}^{3/2}).$$

We should stress that the above expansions are strictly valid only when $\chi = 1$. From these expressions, it is easy to see that the two components of the base-state stress, F_{o11} and F_{o12}, are $O({C_I}^{1/2})$ while F_{o22} is $O(C_I)$. When these terms are incorporated in the linearized equations of Appendix C, one can show that the two components of

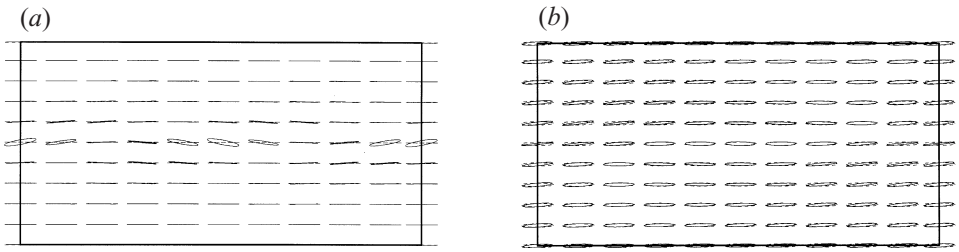

FIGURE 7. Distribution of the fibre orientation in the flow: (*a*) $C_I = 0$; (*b*) $C_I = 0.01$.

the second-order orientation tensor perturbation are

$$a_{11} \sim -2C_I \frac{\psi'' + \alpha^2\psi}{\mathrm{i}\alpha U_o + \sigma}, \quad a_{12} \sim \frac{\alpha^2\psi}{\mathrm{i}\alpha U_o + \sigma}.$$

These expressions show that, for very small or zero orientational diffusivity, a fibre will be simply rotated to align with the displaced streamline. The angle of rotation is given by a_{12}, which in the shear layer where U_o is very small, is given by $\alpha^2\psi/\sigma$. Far from the shear layer, the rotation decays rapidly.

The previous results can be further understood by comparing the final orientation with the base-state orientation. For this purpose, we examine the spatial orientation distribution of the fibres for $C_I = 0.01$ and $C_I = 0$, and for $H = 3.31$. For a given second-order orientation tensor $\boldsymbol{a_2}$, we determine its eigenvectors and eigenvalues, which indicate the orientation directions in the plane of the flow and the degree of alignment with respect to these directions. Hence, we can represent the orientation of a fibre by an ellipse whose major axes are determined by the eigenvectors and the eigenvalues of $\boldsymbol{a_2}$, giving the direction and size of each axis, respectively.

Figures 7(*a*) and 7(*b*) show the base-state orientation of the fibres as dotted lines and the final orientation resulting from the perturbation as solid lines. The final orientation has been defined here arbitrarily as the base state augmented with 10% of the perturbation $\boldsymbol{a_2}$. Therefore it is not possible to draw any quantitative conclusions from these figures. However, one can get some general qualitative trends that indicate how the fibre orientation is changed in the flow. Given the high aspect ratio considered in this analysis, the fibres are initially aligned with the flow when hydrodynamic interactions are ignored (dotted lines in figure 7*a*). In the presence of the perturbation (solid lines), we see that only particles within the shear layer experience a strong misalignment while those in the quiescent flow outside the shear layer remain aligned in the streamwise direction. In the case where C_I is non zero, the base-state orientation shows some misalignment from the streamwise direction. Then the perturbation induces a change in the particle orientation that propagates far beyond the shear layer and affects the orientation of the particles everywhere in the flow (figure 7*b*).

From the previous observations about the streamfunction and the orientation tensor disturbances, we conclude that, due to inter-particle hydrodynamic interactions, the orientation disturbance is not limited to the shear layer, but propagates outside this region. As a consequence, the velocity perturbation is more diffuse and spreads outside the shear layer. As we discussed earlier, such spatial distribution tends to weaken the flow instability. On the other hand, when hydrodynamic interactions are disregarded, the orientation disturbance is confined within the shear layer where the fibres are aligned with the streamlines. This leads to a stronger velocity field disturbance in

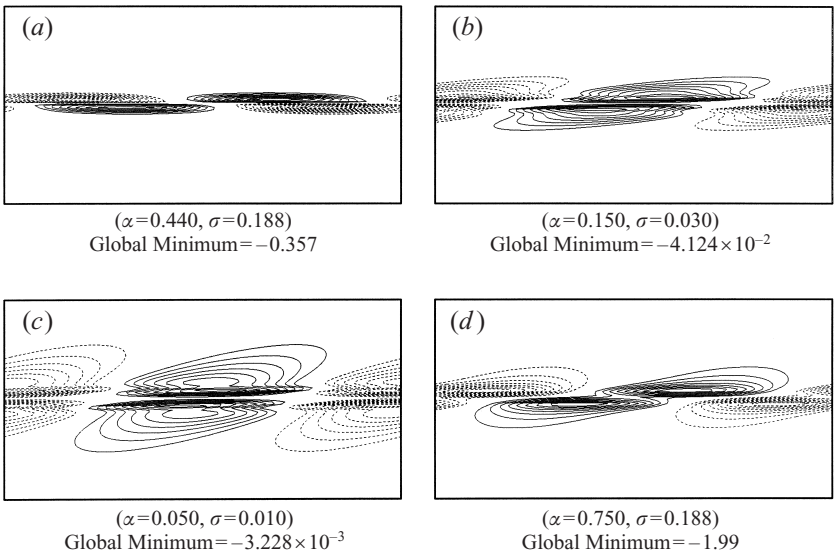

FIGURE 8. Contours of rate of production of vorticity disturbance at the maximum growth rate. (*a*) Newtonian fluid ($H = 0$); (*b*) $H = 3.31, C_I = 0.01$; (*c*) $H = 6.61$, $C_I = 0.01$; (*d*) $H = 3.31$, $C_I = 0$.

a region where the base-state velocity $U_o = \tanh(y)$ is almost zero, and therefore enhances the instability of the flow.

5.3.1. *Vorticity production*

More insight into the effects of the presence of fibres on the flow instability can be gained by examining the spatial distribution of different disturbance quantities. The most important physical quantity to study in this type of flow is the vorticity. Therefore, we will examine in detail the different terms appearing in the vorticity equation:

$$\left(\frac{\partial}{\partial t} + U_o\frac{\partial}{\partial x}\right)\omega = -v\omega_o' + \frac{1 + C\phi}{Re}\nabla^2\omega + H\left[\left(\frac{\partial^2}{\partial x^2} - \frac{\partial^2}{\partial y^2}\right)F_{12} + \frac{\partial^2}{\partial x \partial y}(F_{22} - F_{11})\right]. \tag{28}$$

In what follows we show contours of different terms involved in the production of the vorticity disturbance. Values of the global minimum are indicated and will be used to determine the relative importance of each term for a given type of fluid. For brevity we will not present results for the term $(1 + C\phi)\nabla^2\omega/Re$, since its contribution to the vorticity production is negligible and can be ignored.

The results are presented for one wavelength $\lambda = 2\pi/\alpha$ in the streamwise direction, while the extent of the domain in the transverse direction has been limited to $-60 \leqslant Y \leqslant 60$, even though the numerical solutions of the eigenvalue problems have been carried out for larger values of Y. For easy comparisons, eight solid-line contours are used to represent positive values of a disturbance function F between its (positive) maximum F^+_{max}, and 20% of F^+_{max}. Similarly, eight dotted-line contours are used to represent negative values of F.

Figure 8 shows the rate of accumulation of the vorticity for four types of fluid. We see that in the limit of a Newtonian fluid, there are two distinct regions. First in the downstream half-wavelength, the rate of production of vorticity is negative in the

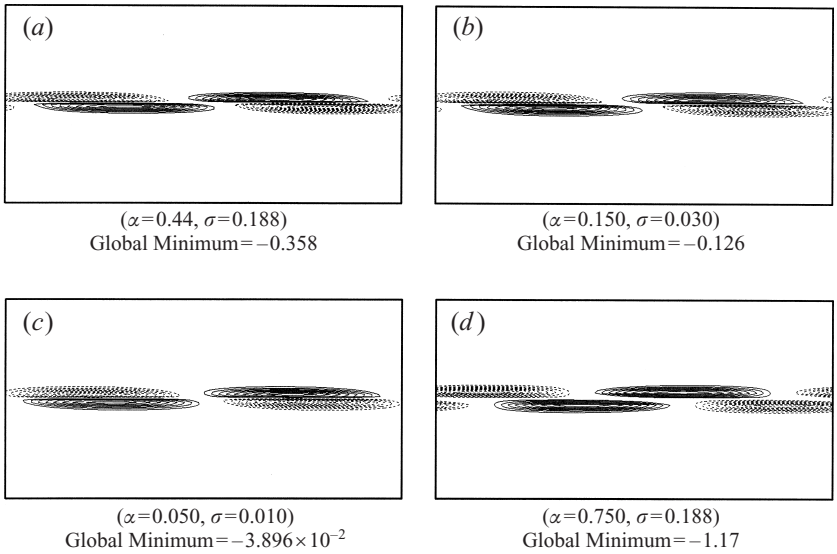

FIGURE 9. Contours of $-v\omega_o'$ at the maximum growth rate. (*a*) Newtonian fluid ($H = 0$); (*b*) $H = 3.31$, $C_I = 0.01$; (*c*) $H = 6.61$, $C_I = 0.01$; (*d*) $H = 3.31$, $C_I = 0$.

lower part of the flow and positive in the upper one. This corresponds to a depletion of vorticity in the upper flow and an increase in the lower flow. Keeping in mind that the base-state vorticity is negative, we conclude that the upper flow has a higher vorticity than the lower one and tends to roll into the lower part. The opposite trend is taking place in the upstream half-wavelength where the lower part of the flow tends to roll into the upper part. This distribution of the vorticity disturbance sets the stage for the beginning of a roll-up of the upper stream around the lower one.

The addition of fibres with hydrodynamic interactions ($C_I = 0.01$) leads to a spatial phase shift that reduces the extent of the region where there is a superposition of vorticity production and depletion, therefore weakening the starting of any roll-up. The phase shift is most noticeable in the case $H = 6.61$, where the positive contours in the upper and lower parts of the flow are almost superposed. This phase shift, similar to the one reported for the viscoelastic mixing layer (Azaiez & Homsy 1994*a*), suggests that the mechanisms of reduction of the flow instability by high-aspect-ratio fibres bear some similarities with that of highly viscoelastic polymers. In the case where fibre–fibre interactions are ignored ($C_I = 0$), the presence of fibres in the flow does not lead to any noticeable spatial phase shift.

Figure 9 depicts contours of the convective term $-v\omega_o'$. In the case of the Newtonian fluid, since the contribution of the viscous term to the flow is negligible, the contours are basically identical to those we showed previously for the rate of production of vorticity. The presence in the flow of fibres with non-zero orientational diffusivity induces a phase shift that increases with increasing H, but which is opposite in sign to the one reported earlier for the rate of production of vorticity. On the other hand, when $C_I = 0$, the phase shift is of the same sign as the one observed for the rate of production of vorticity. Based on these observations and our previous interpretation of the role of the phase shift observed in the vorticity production (Azaiez & Homsy 1994*a*), we conclude that the convective term ($-v\omega_o'$) plays a destabilizing role when hydrodynamic interactions are important, while it is less destabilizing in the case of non-interacting fibres.

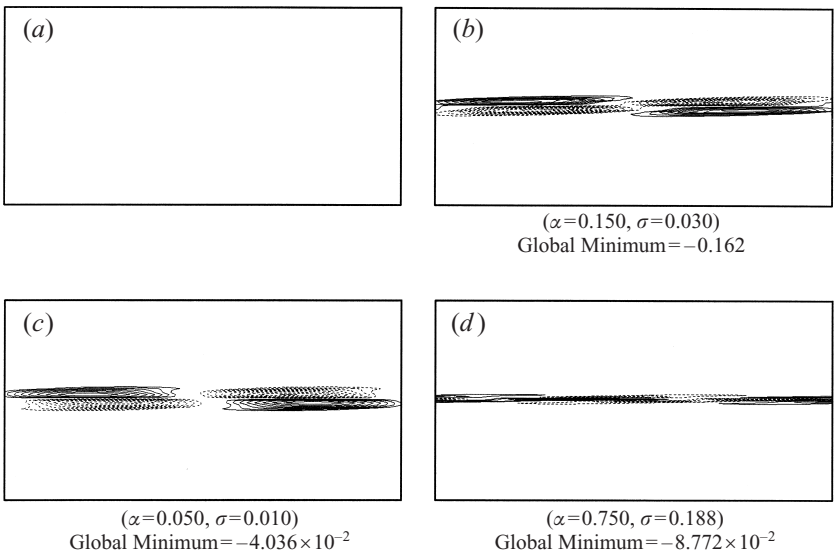

FIGURE 10. Contours of the shear stress contribution to the vorticity production at the maximum growth rate. (*a*) Newtonian fluid ($H = 0$); (*b*) $H = 3.31$, $C_I = 0.01$; (*c*) $H = 6.61$, $C_I = 0.01$; (*d*) $H = 3.31$, $C_I = 0$.

The third term representing the contribution of the shear component of the perturbation stress, $H(\partial^2/\partial x^2 - \partial^2/\partial y^2)F_{12}$, is identically zero in the case of the Newtonian fluid (blank box in figure 10). A close examination of the distribution of the contours in the two cases where interacting fibres are present in the flow reveals an interesting result when these contours are contrasted with the previous ones for the term $(-v\omega_o')$ (see figure 9). In the case of interacting fibres ($C_I = 0.01$), the contours are qualitatively and quantitatively similar to the corresponding contours of $(-v\omega_o')$ (see the general shape of the contours and the values of the global minima). However, there is a major difference in the spatial distribution of the negative and positive contours that suggests that two terms are acting in an opposite way. This result is more clear for $H = 6.61$ where, from the superposition of the positive and negative contours and the values of the minima, one may speculate that the contribution of the fibre shear stress almost cancels out that of the convective term $(-v\omega_o')$. For non-interacting fibres, the contribution of the shear stress disturbance is very small and is mainly confined within the shear layer.

Figure 11 depicts contours of the first normal stress difference perturbation $H(\partial^2/\partial x\partial y)(F_{22} - F_{11})$, which is identically zero for the Newtonian fluid. In the two cases where $C_I \neq 0$, the normal stress contribution to the vorticity production shows an alternation of positive and negative values in the lower and upper parts of the flow. By comparing values of the global minima, we notice that the contribution of this term is always smaller than that of the shear stress component. The general shape of the contours is drastically changed when hydrodynamic interactions are ignored. In this case, the normal stress disturbance extends far beyond the shear layer and shows an alternation of positive and negative values in the lower and upper parts of the flow. Furthermore, its contribution to the vorticity production is much more important than that of the shear stress disturbance, and is of the same order as the contribution of the convective term $(-v\omega_o')$.

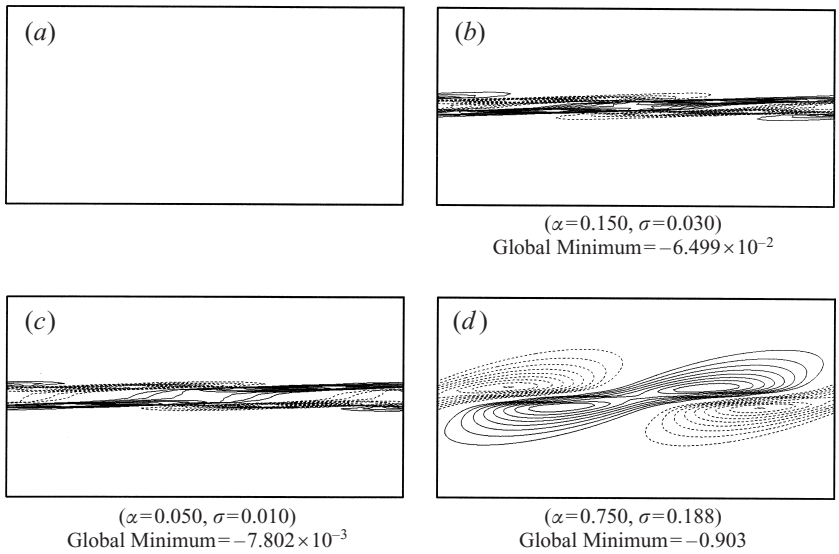

FIGURE 11. Contours of the normal stress contribution to the vorticity production at the maximum growth rate. (*a*) Newtonian fluid ($H = 0$); (*b*) $H = 3.31$, $C_I = 0.01$; (*c*) $H = 6.61$, $C_I = 0.01$; (*d*) $H = 3.31$, $C_I = 0$.

5.3.2. *Energy analysis*

Valuable information about the mechanisms behind the attenuation of the flow instability can be obtained by examining the energy equation for the disturbance. The most common approach consists of using the kinetic energy obtained by taking the scalar product of the linearized momentum equation with the velocity vector, and integrating over the whole domain. Here, we will adopt a different approach based on the enstrophy, defined as the integral of the square of the vorticity. Since the production of vorticity is the key element behind the instability of the flow, we believe that enstrophy is the basic energy quantity for this type of flow. Other forms of disturbance energy such as the kinetic energy must adjust to it.

The equation for the enstrophy balance is obtained by taking the scalar product of the linearized vorticity equation with the vorticity disturbance ω, and integrating over one wavelength and the domain transverse extent $[-\infty, +\infty]$, using the appropriate boundary conditions. This leads to the following equation:

$$\underbrace{\frac{1}{2}\frac{\mathrm{d}}{\mathrm{d}t}\int_0^{\lambda}\int_{-\infty}^{+\infty}\omega^2\,\mathrm{d}y\,\mathrm{d}x}_{ENS} = \underbrace{\int_0^{\lambda}\int_{-\infty}^{+\infty}-v\omega\omega_o'\,\mathrm{d}y\,\mathrm{d}x}_{REW} - \underbrace{\int_0^{\lambda}\int_{-\infty}^{+\infty}\frac{(1+C\phi)||\nabla\omega||^2}{Re}\,\mathrm{d}y\,\mathrm{d}x}_{VIS}$$
$$+\underbrace{H\int_0^{\lambda}\int_{-\infty}^{+\infty}\omega\left(\frac{\partial^2}{\partial x^2}-\frac{\partial^2}{\partial y^2}\right)F_{12}\,\mathrm{d}y\,\mathrm{d}x}_{SHE}$$
$$+\underbrace{H\int_0^{\lambda}\int_{-\infty}^{+\infty}\omega\frac{\partial^2}{\partial x\partial y}(F_{22}-F_{11})\,\mathrm{d}y\,\mathrm{d}x}_{NOR}. \qquad (29)$$

The physical meaning of the different terms in equation (29) can be interpreted as follows. The term ENS represents the rate of change of enstrophy of the disturbance

and is proportional to the growth rate of the disturbance σ. The first term on the right-hand side REW, analogous to the rate of transfer of energy through Reynolds stresses in the kinetic energy equation, is always an energy source. The second term VIS, on the other hand, acts always as an energy sink and represents the rate of dissipation of enstrophy by viscous forces. The last two terms, SHE and NOR, represent the rate of work by the shear and normal stress disturbances, respectively.

The various terms in the equation for the enstrophy have been obtained from the eigenfunction solutions as follows:

$$
\begin{aligned}
ENS &= \pi c_i \mathrm{e}^{2\sigma t} \int_{-\infty}^{+\infty} [(\alpha^2\psi_r - \psi_r'')^2 + (\alpha^2\psi_i - \psi_i'')^2]\,\mathrm{d}y,\\
REW &= \pi \mathrm{e}^{2\sigma t} \int_{-\infty}^{+\infty} [\psi_i(\alpha^2\psi_r - \psi_r'') - \psi_r(\alpha^2\psi_i - \psi_i'')]U_o''\,\mathrm{d}y,\\
VIS &= -\frac{(1+C\phi)}{Re}\frac{\pi \mathrm{e}^{2\sigma t}}{\alpha} \int_{-\infty}^{+\infty} [\alpha^2((\alpha^2\psi_r - \psi_r'')^2 + (\alpha^2\psi_i - \psi_i'')^2)\\
&\quad +(\alpha^2\psi_r' - \psi_r''')^2 + (\alpha^2\psi_i' - \psi_i''')^2]\,\mathrm{d}y,\\
SHE &= H\frac{\pi \mathrm{e}^{2\sigma t}}{\alpha} \int_{-\infty}^{+\infty} [Z12_r(\alpha^2\psi_r - \psi_r'') + Z12_i(\alpha^2\psi_i - \psi_i'')]\,\mathrm{d}y,\\
NOR &= H\frac{\pi \mathrm{e}^{2\sigma t}}{\alpha} \int_{-\infty}^{+\infty} [Z11_r(\alpha^2\psi_r - \psi_r'') + Z11_i(\alpha^2\psi_i - \psi_i'')]\,\mathrm{d}y,
\end{aligned}
$$

where

$$
\begin{aligned}
Z12_r &= L_2\psi_r'' - \alpha(L_{1i}\psi_r' + L_{1r}\psi_i') + \alpha^2(L_{0r}\psi_r - L_{0i}\psi_i),\\
Z12_i &= L_2\psi_i'' + \alpha(L_{1r}\psi_r' - L_{1i}\psi_i') + \alpha^2(L_{0i}\psi_r + L_{0r}\psi_i),\\
Z11_r &= K_2\psi_r'' - \alpha(K_{1i}\psi_r' + K_{1r}\psi_i') + \alpha^2(K_{0r}\psi_r - K_{0i}\psi_i),\\
Z11_i &= K_2\psi_i'' + \alpha(K_{1r}\psi_r' - K_{1i}\psi_i') + \alpha^2(K_{0i}\psi_r + K_{0r}\psi_i).
\end{aligned}
$$

Expressions for the functions K_0, K_1, K_2, L_0, L_1 and L_2 have already been determined in Appendix C. The above integrals have been evaluated at the wavenumber α leading to the maximum growth rate, and are determined at a time $t = 0.5$. In a first stage, we focus on the case of interacting fibres. The role of fibre–fibre interaction will be analysed later.

The variations of the different terms with the parameter H for $C_I = 0.01$ are shown in figure 12. For a pure Newtonian fluid ($H = 0$), the rate of change of the enstrophy production corresponds to the rate of transport of the base-state vorticity by the velocity disturbance and the rate of viscous dissipation, the latter being negligible. When interacting fibres are added to the flow ($H \neq 0$), the picture changes significantly with the presence of two new competing terms associated with the fibre stress disturbance. For these flows, the negative rate of work by shear stresses is opposing the positive contributions from the normal stress difference and the term REW. As H increases and the flow instability is reduced, the rate of enstrophy production starts decreasing. This decrease which is accompanied by a similar, though slower, decay in the energy source term REW, is mainly driven by a sharp increase in the energy sink term SHE. Up to a limiting value $H_L \sim 2.8$, the increase in H induces an increase in the energy source and energy sink associated with the work of the normal and shear stress components respectively. Beyond this value, both contributions start decaying. At large values of H, the main competing

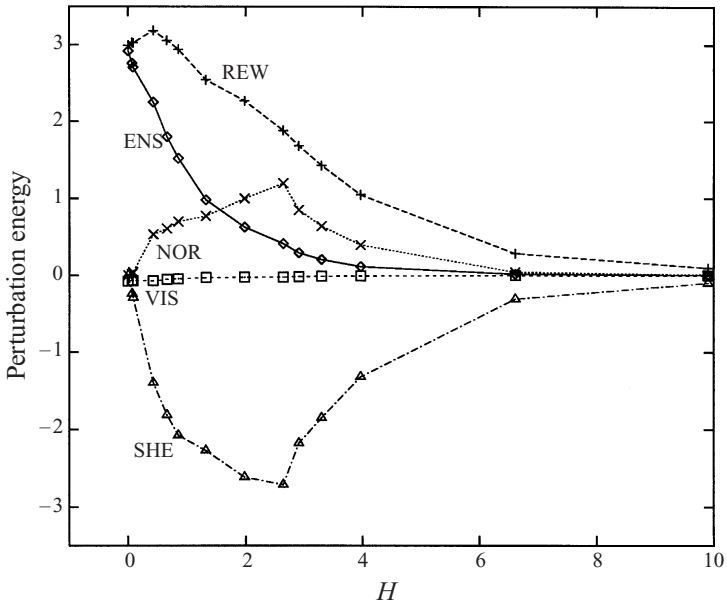

FIGURE 12. Variation of the different terms in the enstrophy equation ($C_I = 0.01$).

Fluid	(α, σ)	REW/ENS %	VIS/ENS %	NOR/ENS %	SHE/ENS %
Newtonian	$\alpha = 0.440, \sigma = 0.188$	102.5	−2.5	0	0
Fibres ($C_I = 0.00$)	$\alpha = 0.750, \sigma = 0.187$	35.6	−6.2	67.2	3.3
Fibres ($C_I = 0.01$)	$\alpha = 0.150, \sigma = 0.030$	692.6	−5.6	311.7	−898.8

TABLE 1. Relative values of different terms in the equation for the rate of change of enstrophy: $H = 3.31$, $Re = 10^3$

terms that are left are those associated with the shear stress work and the transport of enstrophy by the velocity disturbance, with the former showing a dissipating effect that attenuates the growth of the rate of enstrophy production, while the latter still plays a destabilizing role. This last conclusion confirms our previous interpretation of the role of the different terms involved in the production of vorticity.

In what follows, we turn our attention to the role of hydrodynamic interactions, and present values of the different terms in the enstrophy equation for $C_I = 0.01$ and $C_I = 0$, and for $H = 3.31$. To discuss the effects of C_I, it may be more convenient to present the relative contribution as the percentage of each term of the total rate of production of enstrophy. From table 1, it is evident that when no hydrodynamic interactions are included and the fibres are almost aligned with the flow, the rate of change of production of enstrophy is basically reduced to the sum $(REW + NOR)$ where both terms are positive, and therefore play a destabilizing role. The relative contributions of the two terms SHE and VIS are negligible. The above conclusions clearly support our previous analysis of the contours of the different terms contributing to the production of vorticity. In the absence of orientational diffusivity, the instability is mainly fed by the convection of the base-state vorticity and the growth of fibre normal stresses. The result changes completely when one

takes into account the role of fibre–fibre interactions. In this case, the rate of work by shear stresses which is always negative, becomes the dominant term in the equation for the enstrophy budget. This sink term balances the positive contributions from the normal stress difference and the REW term.

6. Conclusion

We present the results of an investigation of the effects of fibre additives on the temporal instability of the mixing layer. The main assumptions used in the derivation of the equations are that the mean flow is parallel and steady, and that the orientational diffusivity arising from hydrodynamic interactions is isotropic. Furthermore, we have used a natural closure approximation that is valid for a planar orientation and have ignored the possibility of off-plane orientation. A modified Orr–Sommerfeld equation was derived and solved numerically. The major findings of the present analysis are summarized as follows.

First, it was found that for large Reynolds numbers, the flow instability is determined by two parameters: a coefficient C_I that accounts for orientational diffusion arising from inter-particle hydrodynamic interactions; and a dimensionless group $H = A\phi/Re$, where ϕ is the fibre volume fraction, and A a parameter that depends on the fibre properties. The parameter H which accounts for the fibre resistance to stretching along its axis, can be regarded as the inverse of a Reynolds number representing the ratio of the fluid inertial forces and the viscous forces associated with the anisotropic elongational viscosity of the suspension.

Second, a parametric study showed that variation of both parameters can lead to a spectacular reduction of the flow instability, without suppressing it completely. Furthermore, it was shown that it is important to include hydrodynamic interactions in order to see a decrease in the flow instability. This result suggests that the drag reduction effects observed in fibre-laden free shear flows cannot be solely attributed to the anisotropy introduced by the long fibres, as has been speculated before. It also shows that the re-orientation of the fibres induced by hydrodynamic interaction between the particles is the key factor behind the observed attenuation of the flow instability.

Third, it was observed that the different disturbance quantities are mainly localized within the shear layer when hydrodynamic interactions are ignored. On the other hand, accounting for the re-orientation of fibres resulting from hydrodynamic interactions leads to more diffuse profiles in which the disturbances are no longer confined within the shear layer. These disturbances extending beyond the shear layer have negligible contribution to the flow instability.

Fourth, an analysis of contours of different perturbation terms involved in the production of vorticity, and an examination of the budget equation for the rate of production of enstrophy, revealed that the main factor behind the reduction of the flow instability is associated with the fibre shear stress disturbance. This disturbance is important when hydrodynamic interactions are included in the flow, and acts as a dissipative term as the fibres tend to deviate from the fully aligned anisotropic orientation. On the other hand, fibre normal stress disturbances always play a destabilizing role, and dominate the flow in the absence of hydrodynamic interactions. However, their contribution becomes negligible compared to that of the shear stress disturbance when hydrodynamic interactions are accounted for.

Finally, it was concluded that fibre models based on the assumption that particles are fully aligned with the flow and therefore ignore any misalignment induced by hy-

drodynamic interaction, will fail to capture the main physics of the flow. Furthermore the important role of hydrodynamic interactions discovered, leads us to speculate that an anisotropic diffusivity will have even more pronounced effects on the stability of the flow. This issue will be examined in a future study involving numerical simulations of the full nonlinear problem.

Appendix A. Correction to the laminar Newtonian flow for non-interacting fibres

The two-dimensional form of the equations of motion, continuity and the constitutive equations for the second-order orientation tensor are respectively

$$\left.\begin{aligned}
\boldsymbol{D}(u) &= -p_x + \frac{(1+C\phi)}{Re}(u_{xx}+u_{yy}) + H(F_{11,x}+F_{12,y}),\\
D(v) &= -p_y + \frac{(1+C\phi)}{Re}(v_{xx}+v_{yy}) + H(F_{12,x}+F_{22,y}),\\
u_x + v_y &= 0,\\
\boldsymbol{D}(a_{11}) &= -4C_I|\dot{\gamma}|a_{11} + 2a_{11}u_x + 2a_{12}u_y + 2C_I|\dot{\gamma}| - \chi F_{11}\\
&\quad +(\chi-1)[2a_{11}u_x + a_{12}(u_y+v_x)],\\
\boldsymbol{D}(a_{12}) &= -4C_I|\dot{\gamma}|a_{12} + a_{11}v_x + a_{22}u_y - \chi F_{12} + (\chi-1)\frac{(u_y+v_x)}{2},\\
a_{11}+a_{22} &= 1,\\
\boldsymbol{F} &= \dot{\gamma} : \alpha_4.
\end{aligned}\right\} \quad (A\,1)$$

In the above equations we used the subscripts t, x and y to denote differentiation with respect to time and the two space variables, respectively, and the symbol D represents the convective operator $(u\partial_x + v\partial_y)$. The variables in the above equations are already dimensionless. Let us consider the special limit $\chi = 1$, $C_I = 0$, and use the quadratic closure to get the fourth-order orientation tensor α_4 (Cintra & Tucker 1995):

$$a_{ijkl} = a_{ij}\, a_{kl}.$$

This leads to

$$\boldsymbol{F} = \mathrm{tr}\,(\dot{\gamma}\cdot\alpha_2)\alpha_2 = 2\lambda\alpha_2,$$

where $\lambda = [a_{11}u_x + a_{12}(u_y+v_x) + a_{22}v_y]$. In this case we get

$$\left.\begin{aligned}
\boldsymbol{D}(u) &= -p_x + \frac{(1+C\phi)}{Re}(u_{xx}+u_{yy}) + 2H[\lambda_x a_{11} + \lambda a_{11,x} + \lambda_y a_{12} + \lambda a_{12,y}],\\
\boldsymbol{D}(\boldsymbol{v}) &= -p_y + \frac{(1+C\phi)}{Re}(v_{xx}+v_{yy}) + 2H[\lambda_x a_{12} + \lambda a_{12,x} + \lambda_y a_{22} + \lambda a_{22,y}],\\
u_x + v_y &= 0,\\
\boldsymbol{D}(a_{11}) &= 2(a_{11}u_x + a_{12}u_y)(1-a_{11}) - 2(a_{12}v_x + a_{22}v_y)a_{11},\\
\boldsymbol{D}(a_{12}) &= a_{11}v_x + a_{22}u_y - 2(a_{11}u_x + a_{12}(u_y+v_x) + a_{22}v_y)a_{12},\\
a_{11}+a_{22} &= 1.
\end{aligned}\right\} \quad (A\,2)$$

In the mixing layer, we use the following scaling:

$$\left.\begin{aligned}
\epsilon &= \frac{1}{\sqrt{Re}}, \quad x = x, \quad y = \epsilon y, \quad u = u, \quad v = \epsilon v, \quad p = \epsilon^2 p,\\
a_{11} &= a_{11}, \quad a_{12} = \epsilon a_{12}, \quad a_{22} = \epsilon^2 a_{22}.
\end{aligned}\right\} \quad (A\,3)$$

With the above scaling, λ can be written as

$$\lambda = (u_x a_{11} + u_y a_{12}) + \epsilon^2 (v_x a_{12} + v_y a_{22}) = \lambda_0 + \epsilon^2 \lambda_2.$$

The previous equations are recast in the form

$$\left.\begin{aligned}
uu_x + vu_y &= -\epsilon^2 p_x + (1 + C\phi)\epsilon^2 \left(u_{xx} + \frac{u_{yy}}{\epsilon^2}\right) \\
&\quad +2H[\lambda_{0,x} a_{11} + \lambda_{0,y} a_{12} + \lambda_0 (a_{11,x} + a_{12,y})] \\
&\quad +2\epsilon^2 H[\lambda_{2,x} a_{11} + (\lambda_{2,y} a_{12} \lambda_2 (a_{11,x} + a_{12,y})], \\
\epsilon^2 (uv_x + vv_y) &= -\epsilon^2 p_y + (1 + C\phi)\epsilon^4 \left(v_{xx} + \frac{v_{yy}}{\epsilon^2}\right) \\
&\quad +2H\epsilon^2[\lambda_{0,x} a_{12} + \lambda_{0,y} a_{22} + \lambda_0 (a_{12,x} + a_{22,y})] \\
&\quad +2\epsilon^4 H[\lambda_{2,x} a_{12} + \lambda_{2,y} a_{22} + \lambda_2 (a_{12,x} + a_{22,y})], \\
u_x + v_y &= 0, \\
ua_{11,x} + va_{11,y} &= 2(a_{11} u_x + a_{12} u_y)(1 - a_{11}) - 2\epsilon^2 (a_{12} v_x + a_{22} v_y) a_{11}, \\
ua_{12,x} + va_{12,y} &= a_{11} v_x + a_{22} u_y - 2(a_{11} u_x + a_{12} u_y) a_{12} \\
&\quad -2\epsilon^2 (a_{12} v_x + a_{22} v_y) a_{12}, \\
a_{11} + \epsilon^2 a_{22} &= 1.
\end{aligned}\right\} \tag{A 4}$$

We use the similarity variable, $\eta = y/\sqrt{x}$, and take the streamfunction, to the first order, equal to $\psi^o = \epsilon \sqrt{x} f(\eta)$. The corresponding streamwise and transverse velocities are

$$u^o = f'(\eta), \quad v^o = \frac{(\eta f'(\eta) - f(\eta))}{2\sqrt{x}}. \tag{A 5}$$

The next step is the usual tentative expansion of the variables.

$$\left.\begin{aligned}
u &= u^o + \epsilon^2 \frac{A(\eta)}{x} + o(\epsilon^2), \quad v = v^o + \epsilon^2 \frac{B(\eta)}{x\sqrt{x}} + o(\epsilon^2), \\
a_{11} &= h(\eta) - \epsilon^2 \frac{H(\eta)}{x} + o(\epsilon^2), \quad a_{22} = \frac{H(\eta)}{x} + \epsilon^2 \frac{L(\eta)}{x^2} + o(\epsilon^2), \\
a_{12} &= \frac{g(\eta)}{2\sqrt{x}} + \epsilon^2 \frac{G(\eta)}{x\sqrt{x}} + o(\epsilon^2).
\end{aligned}\right\} \tag{A 6}$$

H, h, g and f satisfy the following equations:

$$ff'' + 2(1 + C\phi) f''' = 0, \tag{A 7a}$$

$$(\eta h - g)[(\eta h - g) f''' + (2(\eta h - g)' + h) f''] = 0, \tag{A 7b}$$

$$fh' - 2(1 - h)(\eta h - g) f'' = 0, \tag{A 7c}$$

$$(2g - f')(\eta h - g) + f(g' - h) + (4H - \eta^2 h) = 0, \tag{A 7d}$$

$$h = 1, \tag{A 7e}$$

with the boundary conditions: $f(0) = 0, f'(+\infty) = 1, f'(-\infty) = -1$.

Equations (A 7*a*) and (A 7*b*) are obtained from the x-component of the momentum equation, while equations (A 7*c–e*) are from the evolution equations for the three

components of the second-order orientation tensor. The solution of the above system is given by

$$2(1+C\phi)f''' + ff'' = 0, \quad h = 1, \quad g = \eta, \quad H = \frac{\eta^2}{4}. \tag{A 8}$$

The Newtonian limit is accessible by setting $\phi = 0$ (no fibres) and it is easy to verify that this limit gives the Blasius equation.

If we define g such that $f(\eta) = g((1+C\phi)\eta)$, then g satisfies the Blasius equation and the solution of the differential equation for f can be mapped to the Blasius solution.

Appendix B. Base-state orientation tensor

The equations for the second-order orientation tensor using the two-dimensional natural closure approximation are

$$4C_I a_{11} = (1+\chi-2\chi a_{11})a_{12} + 2C_I, \tag{B 1a}$$

$$4C_I a_{12} = \frac{1+\chi}{2} - a_{11} - \chi(a_{11}a_{22} + a_{12}^2), \tag{B 1b}$$

where $\chi = (r^2-1)/(r^2+1)$. Equation (B 1a) leads to the relation

$$a_{12} = \frac{2C_I(2a_{11}-1)}{1+\chi-2\chi a_{11}}.$$

Let $\beta = 1+\chi-2\chi a_{11}$ which is equivalent to

$$a_{11} = \frac{\chi+1-\beta}{2\chi}, \quad a_{22} = \frac{\chi-1+\beta}{2\chi}, \quad a_{12} = \frac{2C_I(1-\beta)}{\chi\beta}.$$

When we substitute the above expressions in (B 1b) we get the following quartic equation for β:

$$\beta^4 + (16\,C_I{}^2 + \chi^2 - 1)\beta^2 - 16\,C_I{}^2 = 0.$$

The solution is

$$\beta^2 = \frac{1-16C_I^2-\chi^2+\sqrt{\Delta}}{2}, \quad \Delta = (16C_I^2+\chi^2-1)^2 + 64C_I^2.$$

Since $\beta = 1+\chi-2\chi a_{11}$ must be always positive, the only acceptable root is $\beta = \sqrt{\beta^2}$. In summary the components of the base-state second-order orientation tensor are

$$a_{11} = \frac{\chi+1-\beta}{2\chi}, \quad a_{22} = \frac{\chi-1+\beta}{2\chi}, \quad a_{12} = \frac{2C_I(1-\beta)}{\chi\beta},$$

$$\beta^2 = \frac{1-16C_I^2-\chi^2+\sqrt{\Delta}}{2}, \quad \Delta = (16\,C_I^2+\chi^2-1)^2 + 64C_I^2.$$

In the special limit of zero orientational diffusivity, $C_I = 0$, the above expressions reduce to

$$a_{11} = \frac{1}{2} + \frac{1-\sqrt{1-\chi^2}}{2\chi}, \quad a_{22} = \frac{1}{2} - \frac{1-\sqrt{1-\chi^2}}{2\chi}, \quad a_{12} = 0.$$

Appendix C. Derivation of stability equations for the mixing layer of fibre suspension

The linearized equations for the components of the second-order orientation tensor and the vorticity disturbances are

$$\left.\begin{aligned} \mathrm{i}\alpha[V_o(\mathrm{D}^2-\alpha^2)+\omega_o']\psi &= \frac{1+C\phi}{Re}(\mathrm{D}^2-\alpha^2)^2\psi + H[(\mathrm{D}^2+\alpha^2)F_{12} \\ &\quad +\mathrm{i}\alpha\mathrm{D}(F_{11}-F_{22})], \\ C_{11}a_{11}-C_{12}a_{12} &= (\mathrm{i}\alpha C_1\mathrm{D}+\alpha^2C_0)\psi, \\ E_{12}a_{12}-E_{11}a_{11} &= (\mathrm{i}\alpha E_1\mathrm{D}+\alpha^2E_0)\psi, \\ a_{11}+a_{22} &= 0, \end{aligned}\right\} \tag{C 1}$$

where

$$\left.\begin{aligned} H &= \frac{A\phi}{Re}, \quad V_o = U_o - c, \\ C_{11} &= E_{12} = \mathrm{i}\alpha V_o + 4C_I U_o' + 2U_o' a_{o12}, \\ C_{12} &= -E_{11} = [1+\chi(1-2a_{o11})]U_o', \\ C_1 &= 2a_{o11}(1-a_{o11}) + 2a_{o12}^2, \\ C_0 &= -2a_{o12}, \quad E_1 = 2\chi a_{o12}(1-2a_{o11}), \quad E_0 = 2a_{o11}-1, \end{aligned}\right\} \tag{C 2}$$

and $\mathrm{D} = \mathrm{d}/\mathrm{d}y$. Solving for a_{11} and a_{12} leads to the following equations:

$$a_{11} = (\mathrm{i}\alpha N_1\mathrm{D}+\alpha^2N_0)\psi, \quad a_{12} = (\mathrm{i}\alpha M_1\mathrm{D}+\alpha^2M_0)\psi,$$

where

$$\left.\begin{aligned} N_1 &= \frac{C_{11}E_1+E_{11}C_1}{CE}, \quad N_0 = \frac{C_{11}E_0+E_{11}C_0}{CE}, \\ M_1 &= \frac{C_{12}E_1+E_{12}C_1}{CE}, \quad M_0 = \frac{C_{12}E_0+E_{12}C_0}{CE}, \\ CE &= C_{11}E_{12}-E_{11}C_{12}. \end{aligned}\right\} \tag{C 3}$$

From the expression for F in equation (23) we have

$$\left.\begin{aligned} F_{11} &= 2a_{o11}a_{o12}(\mathrm{D}^2+\alpha^2)\psi + 2(a_{o11}^2-a_{012}^2)\mathrm{i}\alpha\mathrm{D}\psi \\ &\quad +2U_o'a_{o11}a_{12} + 2U_o'a_{o12}a_{11}, \\ F_{22} &= 2a_{o22}a_{o12}(\mathrm{D}^2+\alpha^2)\psi + 2(a_{o12}^2-a_{022}^2)\mathrm{i}\alpha\mathrm{D}\psi \\ &\quad +2U_o'a_{o22}a_{12} - 2U_o'a_{o12}a_{11}, \\ F_{12} &= (a_{o11}a_{o22}+a_{o12}^2)(\mathrm{D}^2+\alpha^2)\psi + 2a_{o12}(2a_{o11}-1)\mathrm{i}\alpha\mathrm{D}\psi \\ &\quad +2U_o'a_{o12}a_{12} + U_o'(2a_{o11}-1)a_{11}. \end{aligned}\right\} \tag{C 4}$$

Substituting in the expressions of a_{11} and a_{12}, we get

$$F_{11}-F_{22} = (K_2\mathrm{D}^2+\mathrm{i}\alpha K_1\mathrm{D}+\alpha^2K_0)\psi, \quad F_{12} = (L_2\mathrm{D}^2+\mathrm{i}\alpha L_1\mathrm{D}+\alpha^2L_0)\psi,$$

where

$$\left.\begin{aligned}
&K_2 = 2a_{o12}(2a_{o11}-1),\\
&K_1 = 2(a_{o11}^2 + a_{o22}^2 - 2a_{o12}^2) + U_o'[knN_1 + kmM_1],\\
&K_0 = 2a_{o12}(2a_{o11}-1) + U_o'[knN_0 + kmM_0],\\
&L_2 = a_{o11}a_{o22} + a_{o12}^2, \quad L_1 = 2a_{o12}(2a_{o11}-1) + U_o'[lnN_1 + lmM_1],\\
&L_0 = a_{o11}a_{o22} + a_{o12}^2 + U_o'[lnN_0 + lmM_0],\\
&kn = 2(2a_{o11}-1), \quad km = 4a_{o12}, \quad ln = 2a_{o12}, \quad lm = (1-2a_{o11}).
\end{aligned}\right\} \tag{C 5}$$

Using the above expressions in the linearized vorticity equation leads to the following modified Orr–Sommerfeld equation:

$$\sum_{i=0}^{4} J_i \mathrm{D}^i \psi = 0, \tag{C 6}$$

$$\begin{aligned}
J_0 &= H[\alpha^2 L_0'' + \mathrm{i}\alpha^3 K_0' + \alpha^4 L_0] + \mathrm{i}\alpha^3 V_o + \mathrm{i}\alpha U_o'' + \alpha^4 \frac{1+C\phi}{Re},\\
J_1 &= H[\mathrm{i}\alpha L_1'' + \alpha^2(2L_0' - K_1') + \mathrm{i}\alpha^3(L_1 + K_0)],\\
J_2 &= H[\mathrm{i}\alpha(2L_1' + K_2') + \alpha^2(L_0 + L_2 - K_1) + L_2''] - \mathrm{i}\alpha V_o - 2\alpha^2 \frac{1+C\phi}{Re},\\
J_3 &= H[2L_2' + \mathrm{i}\alpha(L_1 + K_2)],\\
J_4 &= HL_2 + \frac{1+C\phi}{Re}.
\end{aligned}$$

REFERENCES

Arranaga, A. B. 1970 Friction reduction characteristics of fibrous and colloidal substances. *Nature* **225**, 447–449.

Ascher, U. M., Mattheij, R. M. M. & Russel, R. D. 1988 *Numerical Solution of Boundary Value Problems for Ordinary Differential Equations*. Series in Computational Mathematics. Prentice Hall.

Azaiez, J. 1993 Instability of Newtonian and non-Newtonian free shear flows. PhD Thesis, Stanford University.

Azaiez, J. & Homsy, G. M. 1994*a* Linear stability of free shear flow of viscoelastic liquids. *J. Fluid Mech.* **268**, 37–69.

Azaiez, J. & Homsy, G. M. 1994*b* Numerical simulation of non-Newtonian free shear flows at high Reynolds numbers. *J. Non-Newtonian Fluid Mech.* **52**, 333–374.

Batchelor, G. K. 1970 The stress system in a suspension of force-free particles. *J. Fluid Mech.* **41**, 545–570.

Batchelor, G. K. 1971 The stress generated in a non-dilute suspension of elongational particles by pure straining. *J. Fluid Mech.* **46**, 813–829.

Berman, N. 1978 Drag reduction by polymers. *Ann. Rev. Fluid Mech.* **10**, 47–64.

Cadot, O. & Lebey, M. 1999 Shear instability inhibition in a cylinder wake by local injection of a viscoelastic fluid. *Phys. Fluids* **11**, 494–496.

Cintra, J. S. & Tucker, C. L. 1995 Orthotropic closure approximation for flow-induced fibre orientation. *J. Rheol.* **39**, 1095–1122.

Draad, A. A. & Hulsen, M. A. 1995 Transition from laminar to turbulent flow for non-Newtonian fluids. In *Advances in Turbulence V* (ed. R. Benzi), pp. 105–110. Springer.

Ericksen, J. L. 1960 Transversely isotropic fluids. *Kolloid Z.* **173**, 117–122.

Filipsson, L. G. R., Torgny Lagerstedt, J. H. & Bark, J. H. 1977 A note on the analogous behaviour of turbulent jets of dilute polymer solutions and fibre suspensions. *J. Non-Newtonian Fluid Mech.* **3**, 97–103.

Folgar, F. P. & Tucker, C. L. 1984 Orientation behaviour of fibres in concentrated suspensions. *J. Reinf. Plast. Comp.* **3**, 98–119.

Gadd, G. E. 1965 Friction reduction characteristics of fibrous and colloidal substances. *Nature* **206**, 463.

Gennes, P.G. de 1990 *Introduction to Polymer Dynamics*. Cambridge University Press.

Giesekus, H. 1962 Elasto-Viskose Flüssigkeeiten für die in stationären schichtströmungen sämtliche normalspannungskomponenten verschieden groß sind. *Rheol. Acta* **2**, 50–62.

Hibberd, M. F., Kwade, M. & Scharf, R. 1982 Influence of drag reducing additives on the structure of turbulence in a mixing layer. *Rheol. Acta* **21**, 582–586.

Hinch, E. J. 1977 Mechanical models of dilute polymer solutions in strong flows. *Phys. Fluids* **20**, S22–S30.

Hinch, E. J. & Leal, L. G. 1975 Constitutive equations in suspension mechanics. Part 1. General formulation. *J. Fluid Mech.* **71**, 481–495.

Hinch, E. J. & Leal, L. G. 1976 Constitutive equations in suspension mechanics. Part 2. Approximate forms for a suspension of rigid particles affected by Brownian rotations. *J. Fluid Mech.* **76**, 187–208.

Hoyt, J. W. 1972 The effect of additives on fluid friction. *Trans. ASME* D: *J. Basic Engng* **94**, 258–285.

Joseph, D. D. 1990 *Fluid Dynamics of Viscoelastic Liquids*. Springer.

Koch, D. L. 1995 A model for orientational diffusion in fibre suspensions. *Phys. Fluids* **7**, 2086–2088.

Kumar, S. & Homsy, G. M. 1999 Direct numerical simulation of hydrodynamic instabilities in two- and three-dimensional viscoelastic free shear layers. *J. Non-Newtonian Fluid Mech.* **83**, 249–276.

Landahl, M. T. 1972 Drag reduction by polymer addition. In *Proc. Thirteenth Intl Congress of Theoretical and Applied Mechanics* (ed. E. Becker & G. K. Mikhailov), pp. 177–199. Springer.

Lee, W. K., Vaseleski, R. C. & Metzner, A. B. 1974 Turbulent drag reduction in polymeric solutions containing suspended fibres. *AIChE J.* **20**, 128–133.

Ling, C. & Reynolds, W. C. 1973 Non-parallel flow corrections for the stability of shear flows. *J. Fluid Mech.* **59**, 571–591.

Michalke, A. 1964 On the inviscid instability of the hyperbolic tangent velocity profile. *J. Fluid Mech.* **19**, 543–556.

Pilipenko, V. N., Kalinichenko, N. M. & Lemak, A. S. 1981 Stability of the flow of a fibre suspension in the gap between coaxial cylinders. *Sov. Phys. Dokl.* **26**, 646–648.

Pinho, F. T. & Whitelaw, J. H. 1990 Flow of non-Newtonian fluids in a pipe. *J. Non-Newtonian Fluid Mech.* **34**, 129–144.

Prager, S. 1957 Stress-strain relations in a suspension of dumbbells. *Trans. Soc. Rheol.* **1**, 53–62.

Rallison, J. M. & Hinch, E. J. 1995 Instability of a high speed submerged elastic jet. *J. Fluid Mech.* **288**, 311–324.

Rahnama, M., Koch, D. L. & Shaqfeh, E. S. G. 1995 The effect of hydrodynamic interactions on the orientation distribution in a fibre suspension subject to simple shear flow. *Phys. Fluids* **7**, 487–506.

Riediger, S. 1989 Influence of drag reducing additives on a plane mixing layer. In *Drag Reduction in Fluid Flows* (ed. R. H. J. Sellin & R. J. Moses), pp. 303–310. Ellis Horwood.

Shaqfeh, E. S. G. & Frederickson, G. H. 1990 The hydrodynamic stress in a suspension of rods. *Phys. Fluids* **2**, 7–24.

Squire, H. B. 1933 On the stability of three dimensional disturbances of viscous fluid flow between parallel walls. *Proc. R. Soc. Lond.* A **142**, 621–628.

Tiederman W. G. 1990 The effect of dilute polymer solution on viscous drag and turbulent structure. In *IUTAM Symp. on Structure of Turbulence and Drag Reduction* (ed. A. Gyr), pp. 187–200. Springer.

Vaseleski, R. C. & Metzner, A. B. 1974 Drag reduction in the turbulent flow of fibre suspensions. *AIChE J.* **20**, 301–306.

Verleye, V. & Dupret, F. 1993 In *Developments in non-Newtonian Flows; Proc. 1993 ASME Winter Annual Meeting, Nov. 28–Dec. 3 1993, New Orleans, LA, USA*, Vol. 175, pp. 139–163.